Chapter 6A. Summary of the Dusar-Shaida Copper and Tin Area of Interest

Contribution by Robert D. Tucker, Klaus J. Schulz, and Stephen G. Peters

Abstract

We summarize and interpret results for the Dusar volcanogenic massive sulfide, Shaida porphyry copper, and Misgaran tin skarn subareas of interest. These subareas have been surveyed by joint geologic and compilation activities conducted between 2009 and 2011 by the U.S. Geological Survey (USGS), the U.S. Department of Defense Task Force for Business and Stability Operations, and the Afghanistan Geological Survey. Accompanying our summary are complementary chapters 6B and 6C that address the hyperspectral data and geohydrologic assessments, respectively, of the subareas. In addition, supporting data for this chapter are available at the Ministry of Mines Data Center in Kabul.

The Dusar subarea includes a volcanic-hosted base-metal mineral occurrence with similar characteristics to volcanogenic massive sulfide deposits. In addition to mineralized volcanic rocks, the Dusar subarea is known for its many massive gossans highly prospective for arsenic, zinc, and lead. The Shaida subarea is a volcanic-hosted copper-lead-zinc mineral occurrence having characteristics similar to those of porphyry copper deposits. The subarea was the scene of former mining, and is regarded as highly prospective for future development into a small- to medium-sized operation. The Misgaran subarea, which was not surveyed extensively by USGS scientists, is assessed from historical accounts to be a tin prospect of high potential. Modern geophysical surveys, including low elevation aeromagnetic and aeroradiometric flights, are crucial for understanding the economic potential of these subareas.

6A.1 Introduction

The Dusar-Shaida-Misgaran copper and tin area of interest (AOI) is located in west central Afghanistan (fig. 6A–1), and contains three subareas: Dusar, Shaida, and Misgaran. Each of these subareas is characterized by its distinctive mineral association and geologic setting (Abdullah and others, 1977; Afghanistan Geological Survey, 2006; Peters and others, 2007). The Dusar subarea, in the west, is known for its anomalous concentrations of copper, zinc, and rare gold in siliceous limonitic gossans associated with metamorphosed volcanic rocks, and has been interpreted as a possible volcanogenic massive sulfide deposit. The Shaida subarea, in the central part of the province, is known for its abundant copper and zinc, in massive veinlets and disseminated ore, within altered volcanic strata intruded by small Oligocene granitoids; it has been interpreted as a copper porphyry deposit. The Misgaran subarea, in the east, is noteworthy for its abundant skarn and polymetallic veins enriched in tin and lead, and has been interpreted as a tin skarn deposit.

In August 2010, U.S. Geological Survey (USGS) scientists led a brief 2-day scoping mission to the Dusar, Shaida, and Misgaran subareas. This chapter summarizes the published and unpublished work regarding the economic geology of the subareas, as well as a brief summary of new analytical data and the potential for future discoveries.

6A.2 Metallogeny

Mineral deposits related to felsic-to-intermediate porphyritic igneous rocks in Afghanistan include porphyry copper and associated deposits, such as polymetallic skarns and veins, and gold-bearing parts of the same systems. Many igneous-related copper prospects are located in western and southern Afghanistan in the Farah Rod, Helmand, Arghandab, Spin Boldak, and Chaigi plutonic belts,

northwest of the Chaman fault and south of the Har-i-Rod Fault. Farah Rod is the primary area in Afghanistan that contains known mineral occurrences and geologic features considered promising for future discovery and exploitation of copper-tin-zinc deposits (United Nations Economic and Social Commission for Asia and the Pacific, 1995).

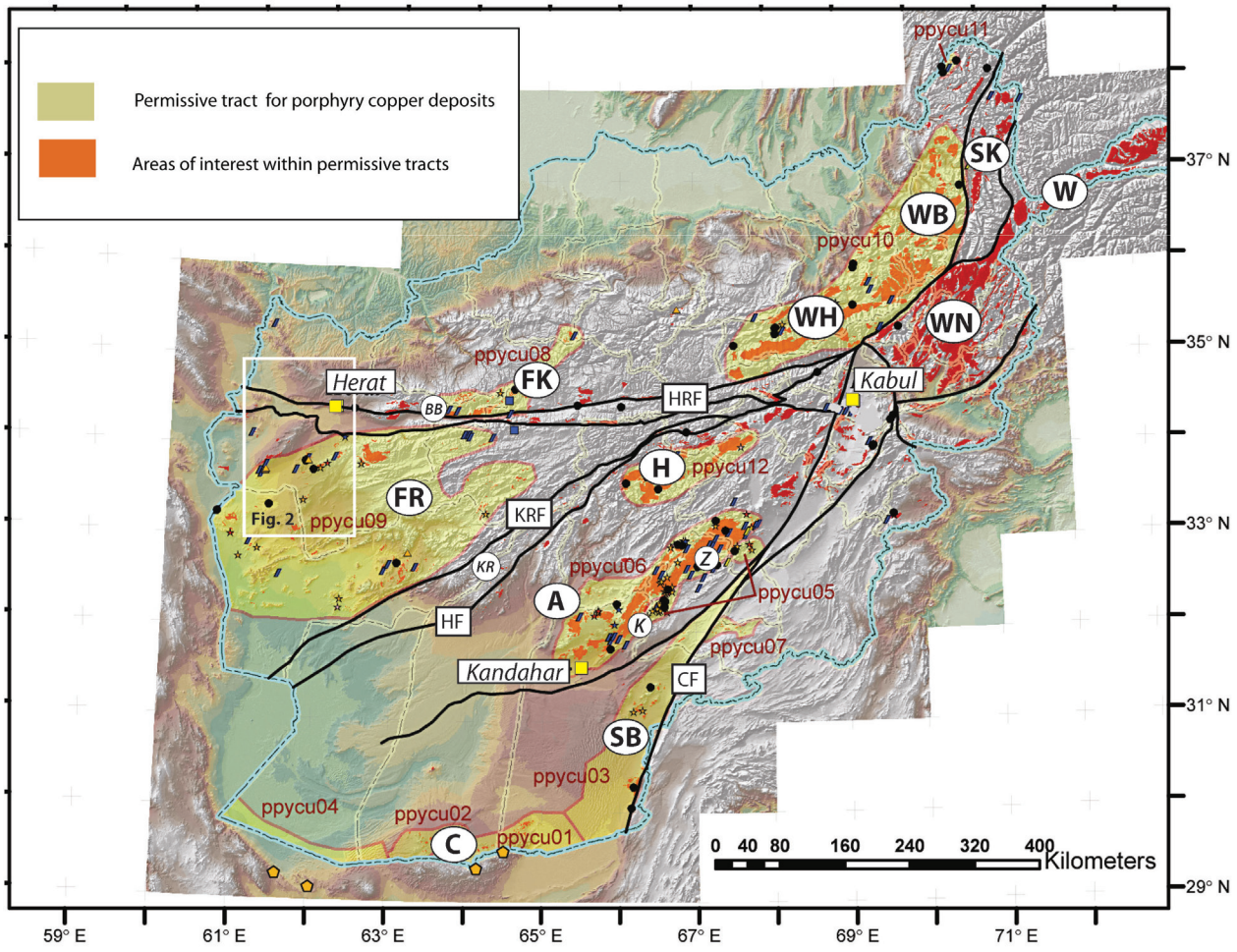

Figure 6A–1. The principal belts of Tethyan calc-alkaline igneous rocks and the areas permissive for porphyry copper and porphyry copper-gold and associated plutonic deposits in Afghanistan (from Peters and others, 2007). Dusar-Shaida-Misgaran area of interest is in the western part of the porphyry copper tract (ppycu09) south of Herat (see fig. 6A–2). Names of the calc-alkaline igneous belts are indicated in oval: A, Arghandab; C, Chagai; FK, Feroz Koh; FR, Farah Rod; H, Helmand; SB, Spin Boldak; SK, Safed Khers; W, Wakhan; WB, West Badakhshan; WH, West Hindukush; WN, West Nuristan. Major faults are in squares: CF, Chaman Fault; HF, Helmand Fault; HRF, Har-i-Rod Fault; KRF, Kash Rud Fault. Significant ore districts are circled: BB, Band-e-Bayan; K, Kundalan; Z, Zarkashan.

About 200 igneous-related hydrothermal mineral deposits and occurrences in Afghanistan contain copper as a major commodity. The majority of these are classified as copper skarn (about 50 prospects) and polymetallic vein (about 70 prospects) occurrences (Plotnikov and others, 1968; Abdullah and others, 1977; Orris and Bliss, 2002; Doebrich and others, 2006; Peters and others, 2007). These occurrences and deposits are spatially associated with, and occur in the same geologic environments as, porphyry copper deposits (Singer and others, 2005); thus, their presence is direct evidence that their environments are permissive for porphyry copper deposits. Furthermore, igneous rocks typical of geologic provinces that contain porphyry copper deposits also are common in Afghanistan. Most of the prospective porphyry copper prospects are associated with Cretaceous through

late Tertiary plutonic rocks that lie within a number of igneous belts that are part of Tethyan magmatic arcs. Most younger igneous-related copper prospects, such as Kundalan and Zarkashan, are located in southeastern Afghanistan, but other prospects such as Ban-e Bayan, and the prospects of this report are present in western and southern Afghanistan (fig. 6A–1; Peters and others, 2007).

Porphyry copper deposits are an essential source of copper worldwide, and are found in plutonic rocks in magmatic arcs in North and South America, Europe, Asia, and the southwestern Pacific Ocean. The Tethyan arcs, stretching from the Carpathian Mountains of southern and eastern Europe through East Asia, are the setting for numerous important porphyry copper deposits to the west (Sar Chesmeh, Iran), south (Reqo Diq, Pakistan), and east (Yulong, Tibet) of Afghanistan. Several of these known copper-bearing occurrences, including Dusar and Shaida, are included in the Atlas of Mineral Resources of the United Nations Economic and Social Commission for Asia and the Pacific region, which presents an updated and summarized inventory of the geology and mineral resources of Afghanistan (United Nations Economic and Social Commission for Asia and the Pacific, 1995).

6A.3 Geology

The Farah Rod tract, in western Afghanistan (fig. 6A–1), coincides, with the Farah Rod plutonic belt of Debon and others (1987). The principal igneous rocks in the Farah Rod plutonic belt range in composition from gabbro (basalt) to granite (rhyolite). They constitute a mostly calc-alkaline suite of igneous rocks whose ages range from Late Cretaceous to Oligocene.

The Dusar subarea, located in the western part of (fig. 6A–2), includes a potential volcanogenic massive sulfide deposit (Peters and others, 2007). The Shaida copper-zinc subarea, located in the east-central part of figure 2, includes a number of polymetallic veins and skarns that are best interpreted as a porphyry copper deposit of significant size (United Nations Economic and Social Commission for Asia and the Pacific, 1995). The Misgaran subarea, located in the eastern part of figure 6A–2, includes a polymetallic vein and tin skarn deposit.

6A.3.1 Dusar Subarea

The Dusar subarea is situated between latitudes 33°30' through 34°00'N. and longitudes 61°0' through 61°30'E., approximately 100 kilometers (km) southwest of the city of Herat. The subarea is located within the Farah Rod belt of Cretaceous to Oligocene calc-alkaline igneous rocks which, in general, is characterized by polymetallic veins and copper skarn occurrences. In the Dusar subarea, however, copper mineralization is hosted within stratified volcanic and sedimentary rocks of Late Jurassic to Early Cretaceous age (figs. 6A–3 and 6A–4). Associated with these are extensive gossans, and many stocks and small intrusive bodies of diorite and gabbro of presumed Early Cretaceous age (fig. 6A–4). The sedimentary strata intercalated with the volcanic rocks include shale and siltstone, with thin horizons of conglomerate, limestone, and chert. The volcanic rocks are dominated by mafic varieties (basalt), lesser felsic varieties (rhyolite), and very few rocks of intermediate composition (dacite-andesite). Because the volcanic section is generally poor in igneous rocks of felsic and intermediate composition, and is interlayered with shallow-marine sedimentary rocks, the Dusar subarea has been modeled as a potential volcanogenic massive sulfide deposit (Peters and others, 2007). The mineralized rocks, and the gossans, are unconformably overlain by unconsolidated gravels and sands of Miocene-Pliocene age. Thus, the copper mineralization must be Paleogene or older, and perhaps related to the igneous rocks of Early Cretaceous age. The gossans are noteworthy for their anomalously high concentrations of copper, arsenic, zinc, and lead (table 6A–1).

6A.3.2 Shaida Subarea

The Shaida subarea is located between latitudes 33°40' through 33°50' N. and longitudes 61°40' through 61°50' E., and is approximately 50 km southwest of Herat (fig. 6A–2). Like the Dusar subarea, the Shaida subarea is located within the Farah Rod tract of Cretaceous to Oligocene plutonic igneous rocks.

Stratified rocks of the Shaida district include three different sequences of very different age and lithology (fig. 6A–5). The oldest sequence, of Permian-Carboniferous age, consists entirely of massive, thin-bedded, weakly metamorphosed white limestone. The next younger sequence, of Early Cretaceous to Paleogene age, consists of subgreenschist to greenschist facies metamorphic rocks including chlorite-sericite, phyllite, and schistose porphyroids of volcanic origin (rhyolite and dacite-andesite). Copper mineralization is widespread in these rocks, and it occurs in strongly silicified and limonitic zones up to 100 meters (m) long and 300 m thick. The mineralized zones contain quartz veinlets, with secondary copper minerals and disseminated chalcopyrite, that grade 0.01 to 0.03 weight percent (wt. %) copper, and up to 0.7 wt. % lead (table 6A–2). These zones also contain anomalous concentrations of zinc, molybdenum, lead, and arsenic.

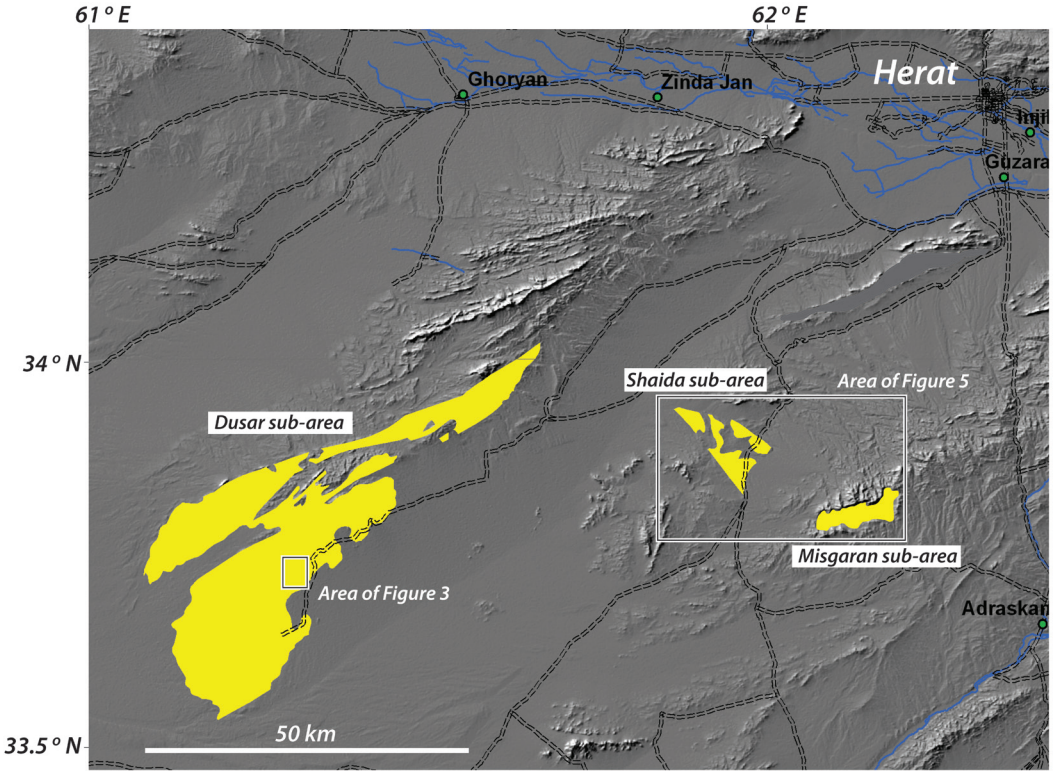

Figure 6A–2. Map showing the location of geologic maps (shown herein) and subareas within the permissive tract of porphyry copper deposits of western Afghanistan. Permissive tracts of copper mineralization are shown in yellow; the permissive tract for the Misgaran tin deposit is not shown; it is indicated only by a label. The outline of figures 6A–3 and 6A–5 are indicated by the white boxes. Figure 1 shows the location of this map in Afghanistan. (Shaded DEM and tracts from Peters and others, 2007.)

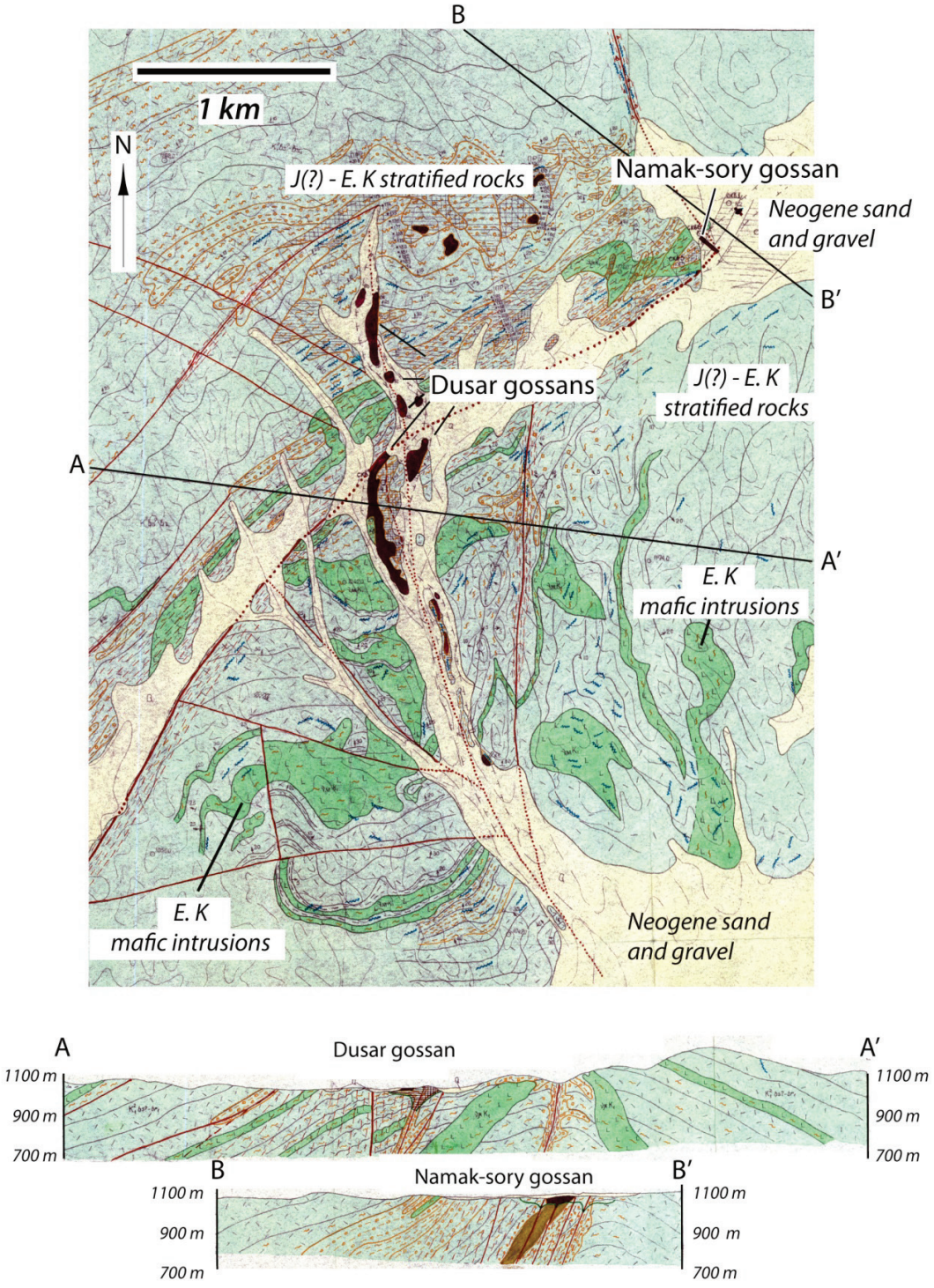

Figure 6A–3. Geology of the Dusar and Namak-sory sites after Tarasenko and others (1973). The prospective volcanogenic massive sulfide (VMS) deposits are situated within uppermost Jurassic(?) to Lower Cretaceous low-grade metasedimentary rocks (shale siltstone, chert, and limestone), including mafic and felsic volcanic strata, intruded by diorite, gabbro, and granodiorite of presumed Early Cretaceous age. Both the Dusar and Namak-sory sites are noted for their prominent “iron caps” of brecciated limonitic gossan, shown in black, that follow prominent north- and northwest-striking fault zones. The gossans and the underlying Lower Cretaceous rocks are overlain unconformably by unconsolidated sand and gravel of Neogene to Recent age.

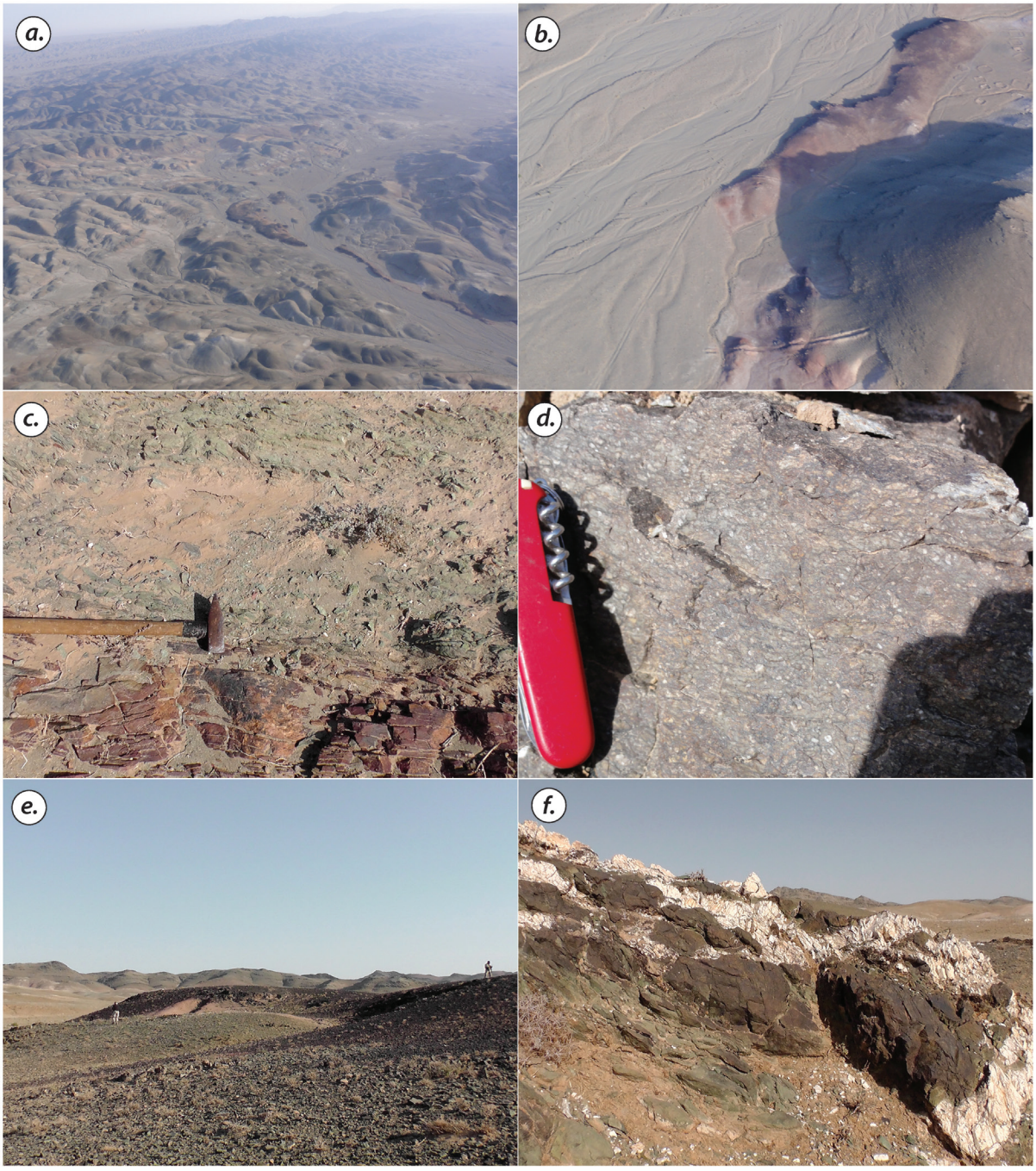

Figure 6A–4. (*a*) Aerial view of the Dusar gossan looking north, (*b*) Aerial view of the Soviet trenches into the Dusar gossan looking north, (*c*) Metabasalt and metachert at the Namak-sory locality, volcanosedimentary rocks, (*d*) Metaquartz keratophyre (metarhyolite) at the Dusar locality, (*e*) View looking north of the Dusar "iron cap" (gossan), (*f*) Close-up of the brecciated and quartz-veined Dusar gossan. Photograph by Robert D. Tucker, U.S. Geological Survey.

Table 6A–1. Major-, trace-, and rare earth element concentration data for whole-rock samples from the Dusar subarea.

[%, percent; ppm, parts per million]

Mineral	Unit	RT–10–D1–1A	RT–10–D1–1B	RT–10–D1–1C	RT–10–D1–02	RT–10–D1–03	RT–10–D2–01	RT–10–D2–02	AC–10–D1–01	AC–10–D1–02
SiO_2[1]	%	56.67	13.04	41.84	11.32	78.95	62.73	75.59	57.53	39.76
Al_2O_3	%	11.26	1.21	2.65	1.76	10.25	8.04	12.03	10.40	2.72
Fe_2O_3	%	7.71	83.88	49.00	85.19	2.78	5.91	3.27	8.10	50.92
MgO	%	5.50	0.27	0.35	0.30	0.50	3.49	1.23	4.53	0.34
CaO	%	13.81	1.28	4.35	0.58	0.97	18.88	0.33	13.88	3.88
Na_2O	%	3.29	0.06	0.93	0.27	4.02	0.10	7.23	4.49	1.22
K_2O	%	0.59	0.03	0.63	0.13	2.08	0.02	0.11	0.12	0.89
TiO_2	%	0.81	0.14	0.03	0.36	0.28	0.44	0.14	0.66	0.03
P_2O_5	%	0.13	0.03	0.17	0.05	0.08	0.12	0.03	0.13	0.20
MnO	%	0.23	0.05	0.04	0.04	0.09	0.26	0.03	0.15	0.05
As	ppm	<1.5	<1.5	90.00	<1.5	<1.5	<1.5	<1.5	<1.5	282.00
Ba	ppm	112.30	150.80	190.20	139.00	514.40	28.40	50.20	35.50	220.40
Be	ppm	0.50	0.10	0.10	0.10	0.90	0.70	1.00	0.30	<0.05
Bi	ppm	0.10	<0.01	0.10	0.00	0.30	0.50	0.40	<0.01	0.30
Cd	ppm	2.40	3.80	1.10	1.00	<0.2	0.30	<0.2	0.30	1.00
Co	ppm	27.60	22.70	7.60	9.80	6.00	10.40	2.50	30.30	10.40
Cr	ppm	151.30	61.80	33.20	87.60	11.80	137.00	6.50	160.30	36.20
Cu	ppm	61.00	336.00	117.00	183.00	17.00	11.00	7.00	39.00	126.00
Ga	ppm	11.10	7.20	32.40	8.40	10.50	9.00	12.10	10.10	35.70
Ge	ppm	0.90	1.00	0.60	1.70	0.90	1.50	0.60	0.60	0.50
Li	ppm	12.40	3.40	7.00	2.40	7.30	3.60	3.90	10.80	7.60
Mo	ppm	0.30	73.50	56.80	11.10	2.00	0.40	3.10	0.30	48.70
Nb	ppm	2.52	0.37	2.46	2.38	10.77	1.82	7.27	2.21	0.35
Ni	ppm	53.20	6.70	4.20	16.20	5.80	37.60	3.70	65.80	4.70
Pb	ppm	6.00	44.70	16.50	31.40	15.50	13.30	3.00	4.40	18.10
S	ppm	85.10	1,388.80	18,046.50	1,457.40	148.10	96.20	151.00	108.80	27,315.50
Rb	ppm	14.10	1.50	4.50	2.80	51.90	1.60	1.70	2.20	5.50
Sb	ppm	0.75	0.02	0.47	0.63	0.85	1.25	0.34	1.15	0.24
Sc	ppm	23.90	2.20	2.50	5.90	6.70	16.50	8.90	20.60	2.40
Sn	ppm	0.70	0.40	0.40	0.60	1.70	0.50	0.90	0.50	0.30
Sr	ppm	138.50	191.10	339.60	89.70	48.40	439.30	55.40	93.10	472.90
Ta	ppm	0.34	0.04	0.01	0.14	1.19	0.11	0.56	0.14	<0.01
Th	ppm	0.60	1.50	1.10	2.80	11.00	0.50	4.30	0.50	1.10
Tl	ppm	0.30	1.00	2.00	0.50	0.30	<0.1	<0.1	<0.1	2.80
U	ppm	0.50	23.60	16.00	19.20	2.60	0.30	1.40	0.20	14.10
V	ppm	208.60	153.70	36.50	190.30	21.70	140.20	9.80	202.00	30.80
W	ppm	<1	<1	<1	<1	1.40	<1	1.20	<1	<1
Y	ppm	26.95	2.10	1.66	3.94	23.87	11.48	33.47	19.87	1.26
Zn	ppm	307.10	1,134.40	1,287.90	1,306.70	30.70	60.50	64.20	85.10	1,068.10
Zr	ppm	45.87	14.16	5.97	34.33	165.65	31.46	174.23	47.33	6.67
Hf	ppm	1.58	0.38	0.27	1.28	5.27	1.05	5.78	1.54	0.18

Mineral	Unit	RT–10–D1–1A	RT–10–D1–1B	RT–10–D1–1C	RT–10–D1–02	RT–10–D1–03	RT–10–D2–01	RT–10–D2–02	AC–10–D1–01	AC–10–D1–02
La	ppm	7.34	3.02	3.24	1.95	26.10	5.16	8.03	5.32	3.34
Ce	ppm	14.22	4.54	1.96	2.95	48.61	8.83	11.31	11.03	1.48
Pr	ppm	2.09	0.50	0.38	0.43	5.47	1.26	2.83	1.84	0.30
Nd	ppm	10.52	1.99	1.46	2.01	21.87	6.24	13.18	8.87	1.68
Sm	ppm	3.13	0.45	0.34	0.56	4.22	1.65	3.60	2.43	0.27
Eu	ppm	1.34	0.07	0.11	0.14	0.76	0.62	0.89	0.94	0.05
Gd	ppm	3.59	0.47	0.47	0.69	4.13	1.53	4.23	2.97	0.51
Tb	ppm	0.72	<0.1	<0.1	0.13	0.75	0.31	0.89	0.51	<0.1
Dy	ppm	4.87	0.42	0.33	0.95	4.79	2.00	6.68	3.51	0.23
Ho	ppm	0.93	0.08	0.07	0.18	0.89	0.43	1.34	0.68	0.04
Er	ppm	2.78	0.21	0.20	0.58	2.80	1.31	4.32	2.31	0.17
Tm	ppm	0.40	<0.04	<0.04	0.09	0.39	0.18	0.65	0.40	<0.04
Yb	ppm	2.57	0.15	0.11	0.70	2.81	1.20	4.84	1.95	<0.1
Lu	ppm	0.36	<0.04	<0.04	0.11	0.44	0.18	0.84	0.29	<0.04

[1]SiO_2 is calculated as = 100 – (Al_2O_3+Fe_2O_3+MgO+CaO+Na_2O+K_2O+TiO_2+P_2O_5+MnO)

Table 6A–2. Major-, trace-, and rare earth element concentration data for whole-rock samples from the Shaida subarea.

[%, percent; ppm, parts per million]

Mineral	Units	FH–10–SD–01	FH–10–SD–02	FH–10–SD–03	FH–10–SD–4/5	FH–10–SD–06	FH–10–SD–07	FH–10–SD–08	FH–10–SD–09	FH–10–SD–10	FH–10–S4–01	FH–10–S4–02
SiO_2*	%	79.69	79.07	32.58	81.04	71.76	66.58	72.23	83.70	92.75	67.34	65.41
Al_2O_3	%	10.67	10.39	3.31	9.66	8.30	21.95	0.46	11.10	2.99	16.42	10.87
Fe_2O_3	%	6.66	3.32	62.41	2.63	14.27	1.22	9.88	2.05	3.29	7.73	22.63
MgO	%	0.61	2.31	0.51	1.16	2.51	0.14	0.16	0.51	0.16	2.99	0.12
CaO	%	0.14	0.54	0.39	0.32	1.00	5.79	16.94	0.38	0.17	0.57	0.32
Na_2O	%	0.09	2.78	0.32	4.56	0.15	1.10	0.08	0.10	0.07	0.15	0.07
K_2O	%	1.99	1.34	0.23	0.42	1.80	2.62	0.11	1.96	0.51	3.82	0.14
TiO_2	%	0.11	0.19	0.03	0.16	0.12	0.46	0.09	0.13	0.03	0.69	0.26
P_2O_5	%	0.02	0.03	0.13	0.02	0.05	0.13	0.04	0.03	0.01	0.26	0.09
MnO	%	0.01	0.04	0.09	0.02	0.03	0.00	0.01	0.04	0.02	0.04	0.09
As	ppm	1,724.00	230.00	313.00	245.00	61.00	646.00	699.00	629.00	369.00	70.00	106.00
Ba	ppm	806.50	347.00	146.10	111.70	496.30	135.70	222.50	373.30	185.80	484.70	71.10
Be	ppm	1.40	1.20	6.60	0.80	1.20	1.00	0.10	0.90	0.40	1.90	1.30
Bi	ppm	4.20	0.30	0.10	<0.01	1.20	41.40	25.70	61.80	0.20	0.30	0.80
Cd	ppm	3.20	2.30	47.40	1.40	12.70	0.50	19.20	1.40	1.20	<0.2	0.50
Co	ppm	7.30	5.70	69.30	3.70	15.50	1.60	2.50	15.00	10.40	16.00	49.10
Cr	ppm	5.60	8.00	3.70	7.10	6.50	20.30	8.00	9.60	611.30	182.10	85.30
Cu	ppm	173.00	615.00	5,845.00	425.00	18,985.50	325.00	139.00	40,847.60	24,912.80	30.00	81.00
Ga	ppm	16.30	14.90	2.30	10.60	13.50	15.20	2.20	15.80	5.80	21.50	10.40
Ge	ppm	1.20	0.80	0.90	0.60	1.00	0.60	0.90	0.80	0.70	1.30	1.10
Li	ppm	19.60	55.10	9.60	23.00	43.70	33.50	3.30	25.10	6.10	84.40	115.40
Mo	ppm	27.00	1.60	61.30	1.70	16.50	33.40	28.20	27.00	7.40	2.10	8.00
Nb	ppm	12.18	8.75	1.84	6.76	9.59	6.70	8.13	11.03	1.33	15.57	5.43
Ni	ppm	4.00	7.10	14.50	4.70	5.00	4.60	5.40	5.20	10.00	53.80	5.40

Mineral	Units	FH–10–SD–01	FH–10–SD–02	FH–10–SD–03	FH–10–SD–4/5	FH–10–SD–06	FH–10–SD–07	FH–10–SD–08	FH–10–SD–09	FH–10–SD–10	FH–10–S4–01	FH–10–S4–02
Pb	ppm	138.00	30.20	37.50	81.70	222.80	1,341.00	1,169.00	1,639.00	6.70	4.30	7.10
S	ppm	218.00	168.00	651.60	139.70	350.40	79,056.90	1,175.80	447.80	237.20	124.50	344.70
Rb	ppm	60.50	46.60	7.60	15.00	47.00	63.20	3.00	65.30	18.00	113.50	6.70
Sb	ppm	4.46	1.14	4.75	0.91	2.01	8.38	17.03	6.94	1.33	0.50	1.53
Sc	ppm	6.60	15.30	2.50	6.60	7.30	18.20	1.40	5.90	3.40	17.00	12.50
Sn	ppm	4.10	2.20	0.50	1.80	3.70	7.00	4.60	18.90	1.20	3.00	1.70
Sr	ppm	128.80	114.60	87.40	117.90	167.50	989.40	182.70	156.80	47.50	57.70	496.70
Ta	ppm	0.94	0.72	0.08	0.40	0.55	0.61	0.16	0.57	0.13	1.07	0.33
Th	ppm	11.20	5.60	1.30	4.60	9.00	8.20	3.40	10.30	1.60	15.30	2.80
Tl	ppm	1.60	0.90	2.10	0.70	1.30	0.40	0.30	5.80	0.20	0.70	<0.1
U	ppm	8.20	1.40	53.90	2.10	56.60	5.70	2.50	66.40	24.40	3.60	6.10
V	ppm	15.60	5.30	15.50	9.00	12.60	98.90	10.90	17.60	37.50	192.20	33.20
W	ppm	1.70	1.00	2.80	1.00	2.20	5.70	1.60	2.00	<1	3.80	3.60
Y	ppm	27.25	43.35	36.55	23.66	29.43	8.06	17.41	35.60	3.89	29.00	24.69
Zn	ppm	938.20	1,772.70	17,890.10	1,647.30	1,630.00	100.10	392.60	148.50	74.50	233.00	1,234.80
Zr	ppm	155.07	160.86	28.51	120.82	140.98	129.27	147.76	150.94	67.46	206.35	82.83
Hf	ppm	5.37	5.35	1.01	4.14	4.48	3.86	4.90	4.71	1.10	6.41	2.62
La	ppm	23.79	27.47	10.45	13.64	23.29	25.00	10.47	27.05	5.19	31.57	16.30
Ce	ppm	46.22	51.20	26.38	24.42	44.11	52.98	18.61	49.20	10.69	64.61	27.83
Pr	ppm	5.09	6.36	4.62	3.21	5.70	6.45	2.16	6.68	1.24	7.58	3.48
Nd	ppm	20.02	28.32	25.46	13.82	23.58	25.73	8.64	30.85	5.34	29.90	15.02
Sm	ppm	4.20	6.80	8.42	3.44	5.70	4.36	1.99	7.02	1.31	6.11	3.59
Eu	ppm	0.65	1.82	2.07	0.64	0.75	0.58	0.36	0.95	0.17	1.41	0.51
Gd	ppm	4.34	6.56	8.61	3.50	4.99	2.75	2.08	6.56	1.11	5.54	3.56
Tb	ppm	0.78	1.26	1.52	0.63	0.88	0.36	0.39	1.09	0.16	0.89	0.61
Dy	ppm	5.38	8.90	9.15	4.68	6.10	1.78	2.85	6.82	1.03	5.69	4.21
Ho	ppm	1.12	1.67	1.59	0.93	1.19	0.36	0.59	1.25	0.18	1.09	0.85
Er	ppm	3.60	5.17	4.61	3.07	3.72	1.06	2.23	3.82	0.61	3.56	2.63
Tm	ppm	0.57	0.77	0.60	0.45	0.55	0.16	0.35	0.52	0.09	0.49	0.35
Yb	ppm	3.77	5.51	4.04	3.42	3.74	1.08	2.93	3.58	0.76	3.47	2.54
Lu	ppm	0.57	0.83	0.55	0.51	0.54	0.19	0.47	0.54	0.11	0.53	0.40

*SiO_2 is calculated as 100 - (Al_2O_3+Fe_2O_3+MgO+CaO+Na_2O+K_2O+TiO_2+P_2O_5+MnO).

Table 6A–2. Major-, trace-, and rare earth element concentration data for whole-rock samples from the Shaida subarea.—Continued

[%, percent; ppm, parts per million]

Mineral	Units	FH–10–S4–03	FH–10–S4–04	FH–10–S4–05	FH–10–S1–01	FH–10–S1–02	RT–10–SD–1A	RT–10–SD–1B	RT–10–SD–1C	RT–10–SD–1D	RT–10–SD–1E	RT–10–SD–1F
SiO_2*	%	91.98	80.36	85.91	79.26	80.63	80.75	80.39	79.59	78.63	17.09	98.23
Al_2O_3	%	2.01	11.47	1.14	9.47	9.64	10.61	9.98	10.53	11.77	0.72	0.13
Fe_2O_3	%	5.46	4.07	10.19	5.51	5.43	4.14	4.41	4.39	1.86	78.72	1.42
MgO	%	0.06	0.51	0.10	1.06	0.16	0.15	0.16	1.60	0.25	0.18	0.08
CaO	%	0.26	0.67	2.19	0.27	0.13	0.35	0.22	0.22	0.96	3.14	0.05
Na_2O	%	0.06	0.10	0.06	0.72	0.18	0.21	0.22	0.92	3.73	0.08	0.05
K_2O	%	0.07	2.57	0.08	3.41	3.64	3.51	4.29	2.55	2.39	0.03	0.01

Mineral	Units	FH–10–S4–03	FH–10–S4–04	FH–10–S4–05	FH–10–S1–01	FH–10–S1–02	RT–10–SD–1A	RT–10–SD–1B	RT–10–SD–1C	RT–10–SD–1D	RT–10–SD–1E	RT–10–SD–1F
TiO_2	%	0.06	0.17	0.02	0.18	0.13	0.20	0.24	0.14	0.33	0.01	0.01
P_2O_5	%	0.02	0.05	0.02	0.05	0.04	0.06	0.08	0.03	0.07	0.03	0.01
MnO	%	0.02	0.02	0.28	0.09	0.02	0.01	0.01	0.02	0.02	0.01	0.01
As	ppm	36.00	<1.5	145.00	85.00	224.00	<1.5	<1.5	<1.5	<1.5	1,423.00	157.00
Ba	ppm	41.90	281.00	202.30	535.10	815.60	775.90	619.80	1,211.90	311.80	4,897.10	28.30
Be	ppm	0.40	1.50	0.80	0.80	1.00	1.30	1.30	1.10	2.80	0.10	<0.05
Bi	ppm	0.20	0.10	0.20	46.60	30.00	0.10	0.10	0.90	0.00	10.50	0.30
Cd	ppm	<0.2	<0.2	0.60	<0.2	<0.2	<0.2	<0.2	0.20	<0.2	2.70	0.10
Co	ppm	9.20	7.70	31.00	33.00	26.80	2.30	2.20	6.80	4.60	2.40	6.50
Cr	ppm	790.60	295.80	595.00	236.20	494.00	239.20	226.80	198.80	285.20	77.30	645.80
Cu	ppm	17.00	36.00	243.00	37,296.70	3,306.00	21,780.90	22,948.90	39.00	46.00	2,196.00	28.00
Ga	ppm	2.20	14.20	1.80	9.50	12.50	11.90	11.20	13.80	15.10	8.60	0.20
Ge	ppm	0.70	1.00	0.60	0.50	1.00	1.30	1.40	0.80	1.20	1.60	0.60
Li	ppm	40.60	35.60	13.50	33.90	27.90	73.90	74.30	50.80	38.40	12.80	1.50
Mo	ppm	2.20	2.40	15.60	1.10	5.20	5.20	5.70	3.90	1.80	115.60	1.60
Nb	ppm	1.58	3.21	0.54	4.01	7.02	8.75	9.86	10.36	10.88	0.46	0.65
Ni	ppm	8.50	4.80	9.00	4.30	7.80	4.70	4.80	3.20	4.80	3.40	8.00
Pb	ppm	3.20	2.70	2.60	66.50	20.60	11.50	12.90	15.60	25.60	1,858.00	3.80
S	ppm	234.00	156.00	321.70	188.10	185.50	465.90	1,000.20	239.80	128.20	3,162.60	177.50
Rb	ppm	4.10	95.00	4.00	124.70	130.10	109.20	139.90	68.00	86.00	1.30	1.50
Sb	ppm	1.33	1.72	8.17	0.41	0.79	0.89	1.01	0.89	0.92	4.17	0.56
Sc	ppm	2.70	7.40	1.40	9.10	3.50	4.20	4.90	12.60	4.30	0.30	<0.1
Sn	ppm	0.50	1.20	0.50	1.20	1.50	3.20	3.60	1.20	4.20	22.50	0.30
Sr	ppm	38.00	54.30	615.00	56.20	56.40	172.60	164.30	228.90	97.40	356.90	5.80
Ta	ppm	0.05	0.44	0.03	0.23	0.89	0.52	0.57	0.47	1.20	0.01	<0.01
Th	ppm	0.60	4.60	0.70	2.10	22.10	11.40	11.50	5.40	26.20	1.20	0.10
Tl	ppm	<0.1	0.70	0.80	1.40	2.00	1.10	1.10	0.70	1.10	<0.1	<0.1
U	ppm	0.90	2.10	4.10	26.90	22.30	45.20	43.20	2.60	3.50	26.70	0.40
V	ppm	12.30	35.10	34.90	34.50	22.00	64.70	51.90	3.50	26.70	225.20	9.50
W	ppm	<1	2.60	<1	2.00	2.00	6.10	7.60	1.40	1.70	2.80	<1
Y	ppm	5.03	8.83	15.65	19.52	22.82	136.80	186.26	49.17	40.93	1.18	0.71
Zn	ppm	375.30	135.40	497.70	60.30	31.70	95.40	104.90	61.20	122.70	925.80	13.10
Zr	ppm	19.37	81.78	14.75	78.39	117.71	248.12	264.50	174.64	264.38	9.40	6.82
Hf	ppm	0.56	2.77	0.45	3.02	4.38	6.30	7.32	5.55	8.23	0.34	0.11
La	ppm	5.98	4.94	10.17	13.94	29.73	17.00	22.22	23.46	36.04	1.68	1.61
Ce	ppm	10.29	8.87	16.51	30.34	60.97	35.45	46.04	45.64	67.39	1.35	2.33
Pr	ppm	1.18	1.02	1.81	3.62	6.73	4.71	6.37	5.58	7.59	0.23	0.28
Nd	ppm	5.28	4.20	8.10	15.71	26.04	26.88	37.77	24.41	28.30	0.99	1.13
Sm	ppm	1.17	0.95	1.97	3.60	5.15	14.55	19.91	6.01	5.39	0.22	<0.2
Eu	ppm	0.14	0.23	0.25	0.85	0.68	2.27	3.02	1.46	0.64	1.71	0.01
Gd	ppm	1.11	1.10	2.49	3.31	4.45	19.55	25.75	6.49	5.18	0.28	0.28
Tb	ppm	0.16	0.19	0.40	0.60	0.71	4.04	5.51	1.25	0.88	<0.1	<0.1
Dy	ppm	0.93	1.46	2.67	3.99	4.72	27.48	38.26	8.84	5.75	0.22	0.15
Ho	ppm	0.22	0.30	0.50	0.75	0.85	5.07	7.05	1.79	1.13	0.04	0.02

Mineral	Units	FH–10–S4–03	FH–10–S4–04	FH–10–S4–05	FH–10–S1–01	FH–10–S1–02	RT–10–SD–1A	RT–10–SD–1B	RT–10–SD–1C	RT–10–SD–1D	RT–10–SD–1E	RT–10–SD–1F
Er	ppm	0.49	1.12	1.27	2.66	2.91	15.46	21.11	5.76	3.62	0.42	0.07
Tm	ppm	0.07	0.17	0.15	0.43	0.42	2.20	3.00	0.79	0.51	<0.04	<0.04
Yb	ppm	0.44	1.44	0.94	2.96	3.02	14.73	21.01	5.66	3.80	<0.1	<0.1
Lu	ppm	0.06	0.23	0.12	0.47	0.43	2.18	2.96	0.88	0.56	<0.04	<0.04

*SiO_2 is calculated as 100 - (Al_2O_3+Fe_2O_3+MgO+CaO+Na_2O+K_2O+TiO_2+P_2O_5+MnO).

Table 6A–2. Major-, trace-, and rare earth element concentration data for whole-rock samples from the Shaida subarea.—Continued

[%, percent; ppm, parts per million]

Mineral	Units	RT–10–SD–1G	RT–10–SD–5A	RT–10–SD–5B	RT–10–SD–5C	RT–10–S4–1A	RT–10–S4–1B	RT–10–S4–1C	RT–10–S1–01	RT–10–S1–02	AC–10–SD–01
SiO_2*	%	80.91	75.42	95.90	35.30	88.96	66.76	78.00	78.25	78.68	80.01
Al_2O_3	%	9.40	0.54	1.35	1.78	0.56	11.59	11.22	9.43	10.96	9.87
Fe_2O_3	%	6.07	13.42	1.23	58.65	9.00	14.31	2.77	5.89	1.72	7.61
MgO	%	0.47	0.12	0.04	0.35	0.16	4.93	1.99	0.95	0.37	0.38
CaO	%	0.61	10.26	1.08	3.62	1.19	0.36	0.48	0.28	0.60	0.28
Na_2O	%	0.09	0.06	0.07	0.07	0.05	0.07	3.64	3.51	3.45	0.11
K_2O	%	2.33	0.08	0.25	0.15	0.03	1.36	1.63	1.31	3.99	1.56
TiO_2	%	0.07	0.06	0.06	0.03	0.01	0.41	0.19	0.19	0.18	0.14
P_2O_5	%	0.03	0.03	0.01	0.03	0.02	0.10	0.05	0.06	0.04	0.02
MnO	%	0.01	0.01	0.02	0.02	0.03	0.10	0.02	0.13	0.02	0.01
As	ppm	91.00	845.00	73.00	2,612.00	<1.5	<1.5	<1.5	<1.5	143.00	373.00
Ba	ppm	568.80	175.00	90.40	497.50	36.70	427.20	234.70	203.30	689.60	225.50
Be	ppm	1.00	0.20	0.40	0.10	0.40	1.40	1.80	0.70	2.60	1.50
Bi	ppm	2.50	5.50	0.20	4.50	0.10	4.70	0.10	0.50	0.20	38.40
Cd	ppm	0.20	2.50	<0.2	3.30	<0.2	<0.2	<0.2	<0.2	<0.2	26.80
Co	ppm	13.10	2.80	2.10	1.90	13.60	25.70	3.80	55.80	2.00	7.50
Cr	ppm	244.50	6.50	10.70	11.20	6.10	17.80	8.40	6.00	9.20	4.40
Cu	ppm	15.00	376.00	23.00	631.00	253.00	64.00	13.00	8,412.00	20.00	50,261.90
Ga	ppm	15.30	1.10	1.60	4.80	1.00	18.80	12.20	10.50	13.80	19.20
Ge	ppm	1.00	1.10	1.00	0.70	0.60	1.00	0.70	0.60	1.00	1.30
Li	ppm	17.90	7.20	10.40	8.30	4.70	192.20	58.80	37.80	16.70	30.20
Mo	ppm	10.00	20.70	1.70	47.90	2.70	1.50	0.30	1.20	0.90	23.00
Nb	ppm	10.25	6.63	2.89	0.84	0.58	11.48	3.86	2.40	7.52	9.98
Ni	ppm	4.40	4.60	4.90	5.10	3.90	8.00	3.80	3.60	4.80	3.20
Pb	ppm	4.90	2,128.00	55.60	216.50	2.50	3.20	4.40	3.80	7.40	442.20
S	ppm	1,978.90	460.80	106.90	1,213.70	115.20	110.40	108.10	97.20	139.30	203.10
Rb	ppm	69.10	2.90	13.20	4.60	1.20	43.60	50.40	58.70	124.30	62.80
Sb	ppm	0.33	25.69	1.41	21.74	2.12	0.51	0.42	0.49	1.41	6.58
Sc	ppm	5.70	0.80	0.80	1.20	0.60	17.30	5.60	9.80	3.00	18.80
Sn	ppm	5.60	3.50	0.70	6.20	0.40	7.40	0.70	2.00	1.00	7.10
Sr	ppm	155.10	79.60	14.20	101.60	27.90	23.90	112.60	60.70	118.80	120.90
Ta	ppm	0.34	0.12	0.18	0.05	0.05	0.90	0.36	0.26	1.28	0.64
Th	ppm	10.90	1.80	2.60	2.10	0.90	7.80	4.20	2.30	25.00	8.70
Tl	ppm	0.50	0.30	0.10	0.40	<0.1	0.40	0.30	0.50	1.20	0.60

Mineral	Units	RT–10–SD–1G	RT–10–SD–5A	RT–10–SD–5B	RT–10–SD–5C	RT–10–S4–1A	RT–10–S4–1B	RT–10–S4–1C	RT–10–S1–01	RT–10–S1–02	AC–10–SD–01
U	ppm	10.50	1.80	0.80	3.20	1.80	3.00	1.50	39.40	3.80	65.60
V	ppm	225.80	24.50	9.90	54.40	8.40	94.40	27.40	27.50	12.10	20.20
W	ppm	1.40	1.50	1.40	1.60	<1	6.60	<1	1.40	1.00	3.00
Y	ppm	24.78	16.26	4.52	1.88	5.63	21.15	12.36	24.46	29.52	32.82
Zn	ppm	43.50	518.70	20.50	1,700.30	492.00	106.70	18.50	95.90	19.50	1,158.10
Zr	ppm	168.50	135.56	46.97	15.01	12.12	162.15	97.11	82.41	164.50	173.68
Hf	ppm	5.06	4.44	1.41	0.40	0.32	4.87	3.15	2.92	5.74	5.48
La	ppm	21.61	5.01	6.67	2.45	7.93	14.89	11.38	12.66	32.71	12.03
Ce	ppm	39.53	7.56	10.99	3.59	12.84	29.46	18.80	51.41	60.67	32.49
Pr	ppm	4.33	0.87	1.33	0.45	1.49	3.57	1.98	3.26	6.64	5.13
Nd	ppm	19.12	3.40	4.54	1.85	6.31	14.08	7.74	14.08	24.84	21.66
Sm	ppm	3.42	0.91	0.80	0.37	1.09	2.88	1.59	3.91	5.14	5.69
Eu	ppm	0.48	0.16	0.17	0.13	0.08	0.23	0.43	0.81	0.52	0.90
Gd	ppm	3.24	1.33	0.69	0.38	1.23	2.73	1.66	3.84	4.90	4.85
Tb	ppm	0.57	0.29	0.11	<0.1	0.18	0.54	0.30	0.73	0.83	0.99
Dy	ppm	4.23	2.63	0.95	0.59	1.01	3.69	2.17	5.09	5.10	6.75
Ho	ppm	0.83	0.53	0.14	0.07	0.18	0.77	0.41	0.93	0.99	1.38
Er	ppm	3.21	1.93	0.54	0.19	0.50	2.61	1.49	2.97	3.50	4.56
Tm	ppm	0.41	0.32	0.07	<0.04	0.06	0.36	0.20	0.44	0.48	0.71
Yb	ppm	2.96	2.33	0.56	0.16	1.90	2.90	1.69	2.91	3.46	5.15
Lu	ppm	0.47	0.47	0.06	<0.04	0.04	0.48	0.30	0.47	0.56	0.87

*SiO_2 is calculated as 100 - (Al_2O_3+Fe_2O_3+MgO+CaO+Na_2O+K_2O+TiO_2+P_2O_5+MnO).

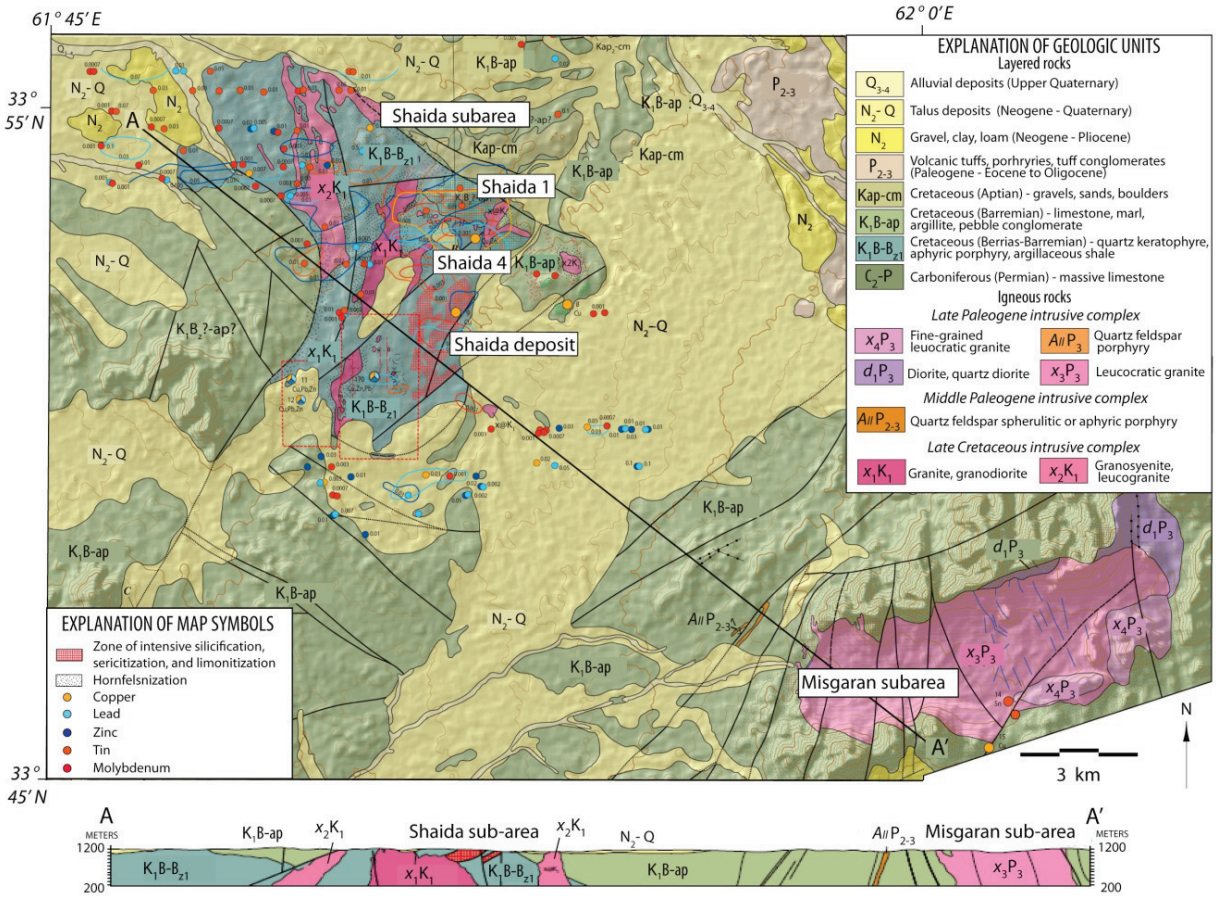

Figure 6A–5. Geologic map and cross section of the Shaida and Misgaran subareas after Tarasenko and others (1973). Localities visited by U.S. Geological Survey scientists are Shaida deposit, Shaida 1, and Shaida 4. All of these sites are within heavily mineralized (copper) volcanic rocks of Early Cretaceous age, as indicated by the cross-hatch pattern (Tarasenko and others, 1973). The line of section, A–A', is also after Tarasenko and others (1973).

Table 6A–2. Major-, trace-, and rare earth element concentration data for whole-rock samples from the Shaida subarea.—Continued

[%, percent; ppm, parts per million]

Mineral	Units	AC–10–SD–02	AC–10–SD–03	AC–10–SD–04	AS–10–SD–02	AS–10–SD–03
SiO_2*	%	77.82	81.66	86.46	87.17	85.71
Al_2O_3	%	11.42	8.57	10.22	6.31	9.67
Fe_2O_3	%	8.76	5.00	1.75	3.34	1.86
MgO	%	0.27	0.72	0.64	0.10	0.41
CaO	%	0.39	0.36	0.54	0.68	0.18
Na_2O	%	0.91	0.33	0.20	0.11	0.08
K_2O	%	0.21	2.36	0.10	2.18	1.98
TiO_2	%	0.12	0.69	0.04	0.07	0.09
P_2O_5	%	0.01	0.25	0.01	0.02	0.02
MnO	%	0.10	0.05	0.04	0.02	0.01
As	ppm	462.00	<1.5	938.00	42.00	565.00
Ba	ppm	50.00	397.10	117.50	487.30	474.00
Be	ppm	0.90	3.50	1.00	0.70	0.60
Bi	ppm	0.50	1.60	11.60	9.20	64.90
Cd	ppm	2.60	0.40	3.80	<0.2	0.40
Co	ppm	61.00	12.60	51.60	20.10	0.60
Cr	ppm	3.50	55.60	4.10	7.20	5.20

Mineral	Units	AC–10–SD–02	AC–10–SD–03	AC–10–SD–04	AS–10–SD–02	AS–10–SD–03
Cu	ppm	27,355.00	35.00	74,258.60	860.00	9,212.00
Ga	ppm	12.00	23.10	10.10	6.50	12.80
Ge	ppm	0.80	2.00	0.80	1.20	1.10
Li	ppm	17.30	54.60	14.10	56.80	21.00
Mo	ppm	207.70	1.40	9.10	5.80	26.80
Nb	ppm	6.99	7.15	4.53	3.19	10.71
Ni	ppm	2.30	26.30	2.00	4.70	3.20
Pb	ppm	23.50	60.70	80.30	14.60	1,846.00
S	ppm	210.30	315.60	727.10	277.30	639.70
Rb	ppm	11.00	141.10	2.50	72.60	53.90
Sb	ppm	3.17	2.17	1.80	1.70	8.91
Sc	ppm	16.80	10.60	8.70	2.20	5.00
Sn	ppm	1.10	9.90	6.60	0.80	18.10
Sr	ppm	271.60	67.40	230.10	63.80	76.20
Ta	ppm	0.44	2.29	0.39	0.42	0.52
Th	ppm	23.00	26.50	11.30	11.60	8.00
Tl	ppm	1.20	1.00	<0.1	1.10	6.00
U	ppm	97.00	5.70	95.40	7.10	23.70
V	ppm	106.00	100.80	44.10	17.90	18.10
W	ppm	2.60	5.70	<1	1.10	1.70
Y	ppm	37.15	20.78	117.42	14.61	36.51
Zn	ppm	1,073.40	101.00	155.20	26.80	69.80
Zr	ppm	132.11	115.07	93.26	76.34	124.72
Hf	ppm	4.03	3.61	2.97	2.83	4.31
La	ppm	2.35	13.22	33.25	15.63	27.37
Ce	ppm	17.20	57.21	101.12	31.36	50.48
Pr	ppm	1.20	3.84	19.11	3.66	5.90
Nd	ppm	7.11	21.21	112.27	14.27	24.29
Sm	ppm	2.57	5.80	29.59	2.93	4.83
Eu	ppm	0.55	0.93	5.00	0.45	0.66
Gd	ppm	3.24	4.41	25.98	2.58	5.04
Tb	ppm	0.86	0.84	4.20	0.47	0.89
Dy	ppm	7.17	5.72	24.79	2.63	5.99
Ho	ppm	1.43	1.09	4.48	0.51	1.24
Er	ppm	4.82	3.78	12.93	1.60	3.99
Tm	ppm	0.75	0.54	1.72	0.23	0.61
Yb	ppm	5.34	4.41	11.71	1.78	4.08
Lu	ppm	0.80	0.69	1.67	0.26	0.68

*SiO_2 is calculated as 100 - (Al_2O_3+Fe_2O_3+MgO+CaO+Na_2O+K_2O+TiO_2+P_2O_5+MnO).

The youngest sequence of strata, of Neogene to Recent age, consists of unconsolidated sand and gravels that unconformably overlie the two older sequences. Their deposition clearly postdates the cycle of volcanic activity in the area (fig. 6A–5).

A small, but significant number of intrusive igneous rocks crop out within the Shaida subarea (fig. 6A–5). These are broadly coeval with the volcanic rocks of Late Cretaceous to Paleogene age. Three phases of intrusive igneous rocks are recognized. First-phase intrusive rocks consist of small stocks and intrusive masses of fine-grained granite and granodiorite (figs. 6A–5 and 6A–6). Second-phase intrusive rocks include leucocratic granosyenite and microcline-rich porphyry granite. These first two phases have been assigned a Late Cretaceous age (Tarasenko and others, 1973). The third and youngest phase of intrusive rocks consists of subvolcanic porphyritic intrusions of Paleocene-Eocene age that range in composition from quartz diorite to granite.

Figure 6A–6. Field photographs of geological relationships and rocks at the Shaida subarea. (*a*) Aerial photograph looking northwest of the Cretaceous intrusive stocks that host the copper porphyry rocks (fig. 6A–5). The stock in the foreground (x1K1) hosts the bulk of the copper mineralization; the stock in the middle ground (x2K2) hosts a second zone of copper mineralization. The ridge in the distant background is outside the area of interest. (*b*) Aerial photograph of modestly dipping, argillaceous shale, sandstone and volcanic strata of Cretaceous age (K1B–Bz1, fig. 6A–5). (*c*) Hand specimen of granite porphyry (x1k1) at the Shaida deposit. (*d*) Copper oxide stained quartz veins in the fractured and brecciated host rock. (*e*) Hematite- and copper oxide-rich leucogranite at the Shaida subarea. (*f*) Iron gossan at the Shaida deposit. Photograph by Robert D. Tucker, U.S. Geological Survey.

The principal zone of copper mineralization at the Shaida subarea is within the volcanic strata of Early Cretaceous age. The volcanic rocks are interstratified with, and overlain by, terrigenous sedimentary rocks that include a thick section of massive, shallow-water limestone, pebbly conglomerate, and clastic redbeds. A continental provenance for the pebbly conglomerates and clastic redbeds is probable. The mineralized volcanic strata are highly fractured and faulted, and intruded by

phase 1 and 2 tabular sheets and stocks of hypabyssal granite porphyry, syenogranite, and leucogranite (Late Cretaceous; Tarasenko and others, 1973). Thus, the Shaida subarea is best considered a deposit of the porphyry-copper type (fig. 6A–5, Peters and others, 2007). The age of mineralization is bracketed between the Paleocene, the age of the porphyritic granitoids that host the deposit, and Pliocene, the age of the gravels that unconformably overlie the deposit.

6A.3.3 Misgaran Subarea

The Misgaran subarea is situated in the southeastern part of figure 6A–5, approximately 16 km southeast of the Shaida subarea. The subarea is defined by three tin-bearing prospects associated with a modest-sized (~ 50 km^2) granite stock of Late Cretaceous age that intrudes Early Cretaceous sandstone and limestone (fig. 6A–7). Two vein and stock prospects are adjacent to the granite stock and are both characterized by quartz-tourmaline mineralization. About 3 km east of the stock is an area of tin-bearing polymetallic veins and tabular skarn beds as much as 50 m thick. The thickness and widespread nature of mineralized rock suggest that these are host to a large polymetallic vein and skarn deposit.

6A.4 Geochemistry

Tables 6A–1 through 6A–3 present major, trace- and rare earth element concentration data for 48 whole-rock samples from the Dusar, Shaida, and Misgaran subareas. Samples include mafic and felsic igneous rocks (intrusive and extrusive), altered and mineralized volcanic strata, as well as gossans, siliceous veins, and minor sedimentary rocks. Because the igneous rocks either intrude or were extruded upon sedimentary rocks of a common sequence (Early to Late Cretaceous), and the igneous rocks are of a common age (Late Cretaceous to Paleocene), we assume that they are genetically related. Our analysis of the geochemical data is a first attempt to understand their genesis and the type of economic mineral deposits associated with them.

Major- and trace-element analyses of the mafic and felsic metaigneous rocks from the Dusar, Shaida, and Misgaran subareas define a calc-alkaline igneous suite ranging in composition from basalt to rhyolite. Based on Soviet-era mapping (Tarasenko and others, 1973), and the observations of our scoping mission, we infer that: (1) igneous rocks of the Shaida and Misgaran subareas are dominated by felsic types (rhyolite, dacite, and granite porphyry), and (2) igneous rocks of the Dusar subarea consist mostly of mafic and intermediate types, with few felsic varieties (quartz keratophyre) (figs. 6A–8 though 6A–10).

In terms of their trace-element abundances, the metaigneous rocks from the three subareas share important similarities and common differences. The metaigneous rocks are generally enriched in the large ion lithophile elements (rubidium, potassium, thorium, and uranium), have significant relative depletions in niobium, tantalum, and titanium, and have strong relative enrichments in lead. In addition, the metaigneous rocks exhibit relatively flat rare earth element (REE) abundance patterns, at 10 to 100 times chondrite abundance, except for the felsic rocks, which show strong relative enrichments in the light REE (LREE; includes lanthanum, cerium, praseodymium, neodymium, and samarium) over the heavy REE (HREE; gadolinium through lutetium). All these characteristics are common to calc-alkaline igneous rocks of subduction origin (figs. 6A–11 and 6A–12). The mafic and felsic metaigneous rocks from Dusar and Shaida have characteristics similar to those of basalts and rhyolites from the Taupo volcanic zone in New Zealand that were emplaced within extended continental crust behind the Hikurangi trench (Balance, 1976; Gamble and others, 1993; figs. 6A–11 and 6A–12). We propose, therefore, that the Late Cretaceous to Paleogene igneous rocks of the Farah Rod belt formed in a continental arc or back-arc setting. This context is consistent with the facies of Lower to Upper Cretaceous sedimentary rocks that host the metaigneous suite.

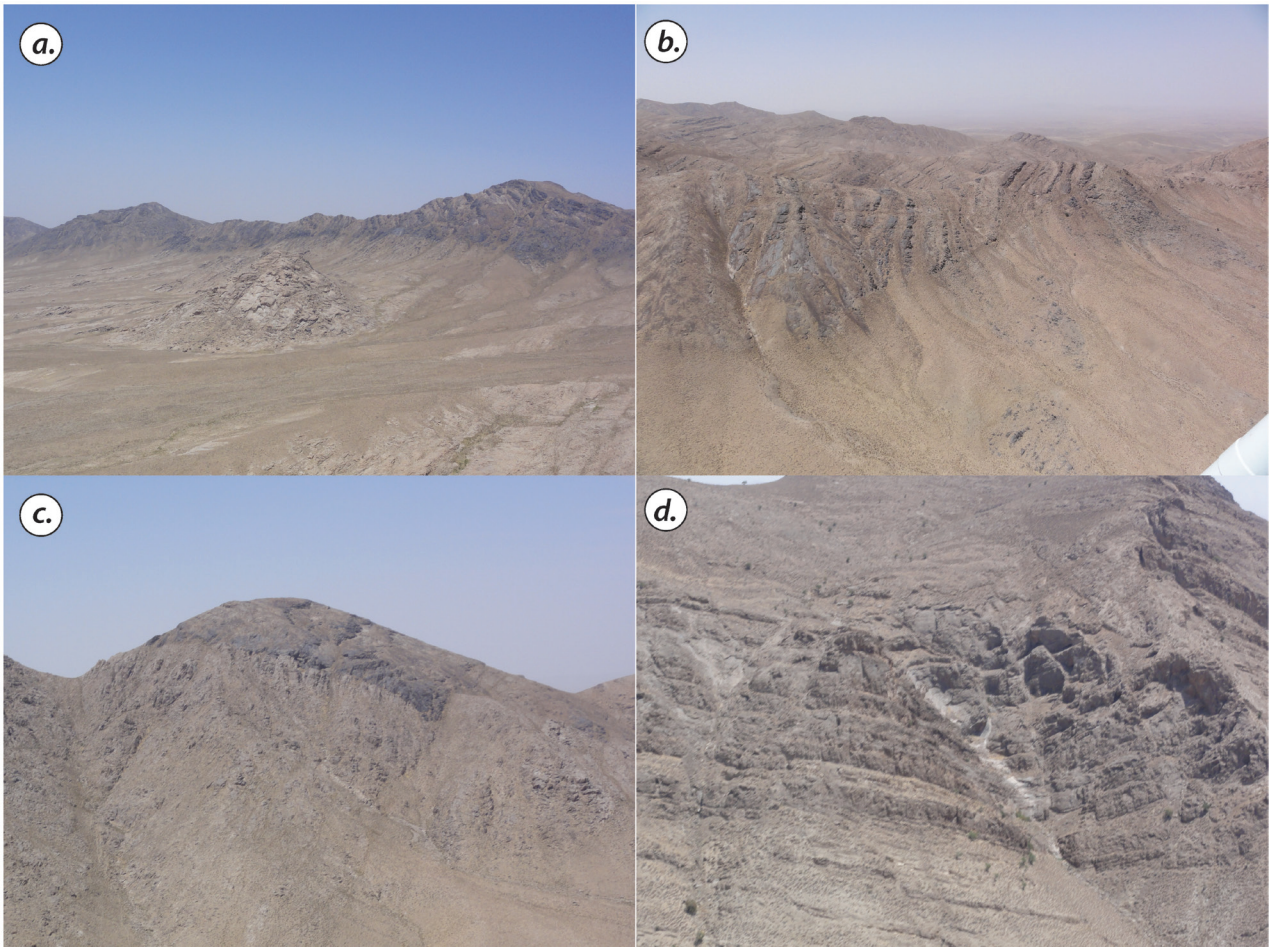

Figure 6A–7. Aerial photographs over the Misgaran subarea and its copper-tin skarn prospects. (*a*) View looking south of the contact skarn showing the contact metamorphosed wall rock (dark colored in background, K1B-ap, fig. 6A–5) and the granite massif (light colored rocks, x3P3, fig. 6A–5) occupying the low foreground. (*b*) View looking south of the hornfels at the southern contact of the granite stock showing the near-vertical dip of contact metamorphosed Cretaceous marl (K1B-ap, fig. 6A–5). (*c*) View looking southwest of brittle deformation of the southern contact aureole showing a few meters displacement along a normal fault. (*d*) View looking south of more brittle deformation of the contact skarn showing quartz-filled gashes in the contact aureole within hornfelsed Cretaceous limestone (K1B-ap, fig. 6A–5). Photograph by Robert D. Tucker, U.S. Geological Survey.

The chemistry of the altered metaigneous rocks and gossans is presented in figure 6A–13. In general, slight to modest alteration of the felsic igneous rocks is accompanied by a decrease in the concentrations of LREEs as well as the alkali elements Rb and K. An increase in alteration results in a decrease in total REE concentrations across their mass range and, in some instances, a pronounced decrease in HREE relative to LREE concentrations. The gossans from Dusar and Shaida have relatively low concentrations of REE (figs. 6A–11 and 6A–12), and in general, relative depletions of cerium, europium, and HREE. These depletions are reflective of leaching by oxidized fluids under supergene conditions (Leroy and Turpin, 1988). For the Shaida rocks, this depletion occurred with a nearly constant ratio of lanthanum to samarium (fig. 6A–12c), suggesting that the gossans are the highly weathered products of the volcanic and (or) metasedimentary rocks. When all bedrock samples, including the gossans, are plotted on the alteration diagram of Large and others (2001), the freshest rhyolites from Shaida plot within the "least altered box" in figure 6A–12d, and the sericitic metavolcanic rocks and argillitic rocks are most enriched in potassium, and depleted in sodium. As might be expected, the gossans are strongly depleted in alkali elements and enriched in ferric iron.

Table 6A–3. Major-, trace-, and rare earth element concentration data of whole-rocks from the Misgaran subarea.
[%, percent; ppm, parts per million]

Sample	Units	RT–10–BM–01	RT–10–BM–02
SiO_2*	%	66.98	69.54
Al_2O_3	%	13.58	12.7
Fe_2O_3	%	5.45	5.11
MgO	%	2.92	1.88
CaO	%	5.07	2.72
Na_2O	%	2.42	3.74
K_2O	%	2.82	3.68
TiO_2	%	0.56	0.43
P_2O_5	%	0.12	0.11
MnO	%	0.09	0.09
As	ppm	<1.5	<1.5
Ba	ppm	302.5	381.2
Be	ppm	1.8	2
Bi	ppm	0.1	0.3
Cd	ppm	<0.2	<0.2
Co	ppm	15.6	10.9
Cr	ppm	48.7	43.2
Cu	ppm	22	26
Ga	ppm	17.8	17.9
Ge	ppm	1	1.4
Li	ppm	55.2	44.7
Mo	ppm	0.9	1.2
Nb	ppm	9.67	9.53
Ni	ppm	15	17.9
Pb	ppm	19.2	21.9
S	ppm	130.2	140.9
Rb	ppm	159.8	138.3
Sb	ppm	0.34	0.78
Sc	ppm	8.9	13.9
Sn	ppm	0.9	5.1
Sr	ppm	55.4	402.9
Ta	ppm	0.56	0.98
Th	ppm	25.1	14.2
Tl	ppm	0.8	0.6
U	ppm	5.2	2.7
V	ppm	99.6	59
W	ppm	2.9	1.9
Y	ppm	23.04	28.69
Zn	ppm	63.1	71.6
Zr	ppm	185.36	198.5
Hf	ppm	6.04	6.27
La	ppm	31.06	33.02
Ce	ppm	60.77	62.44
Pr	ppm	6.74	6.98
Nd	ppm	25.59	27.26
Sm	ppm	5.2	5.44
Eu	ppm	0.95	0.96
Gd	ppm	4.51	4.95
Tb	ppm	0.73	0.83
Dy	ppm	4.32	5.47
Ho	ppm	0.82	1.04
Er	ppm	2.7	3.19
Tm	ppm	0.36	0.47
Yb	ppm	2.35	3.32
Lu	ppm	0.37	0.51

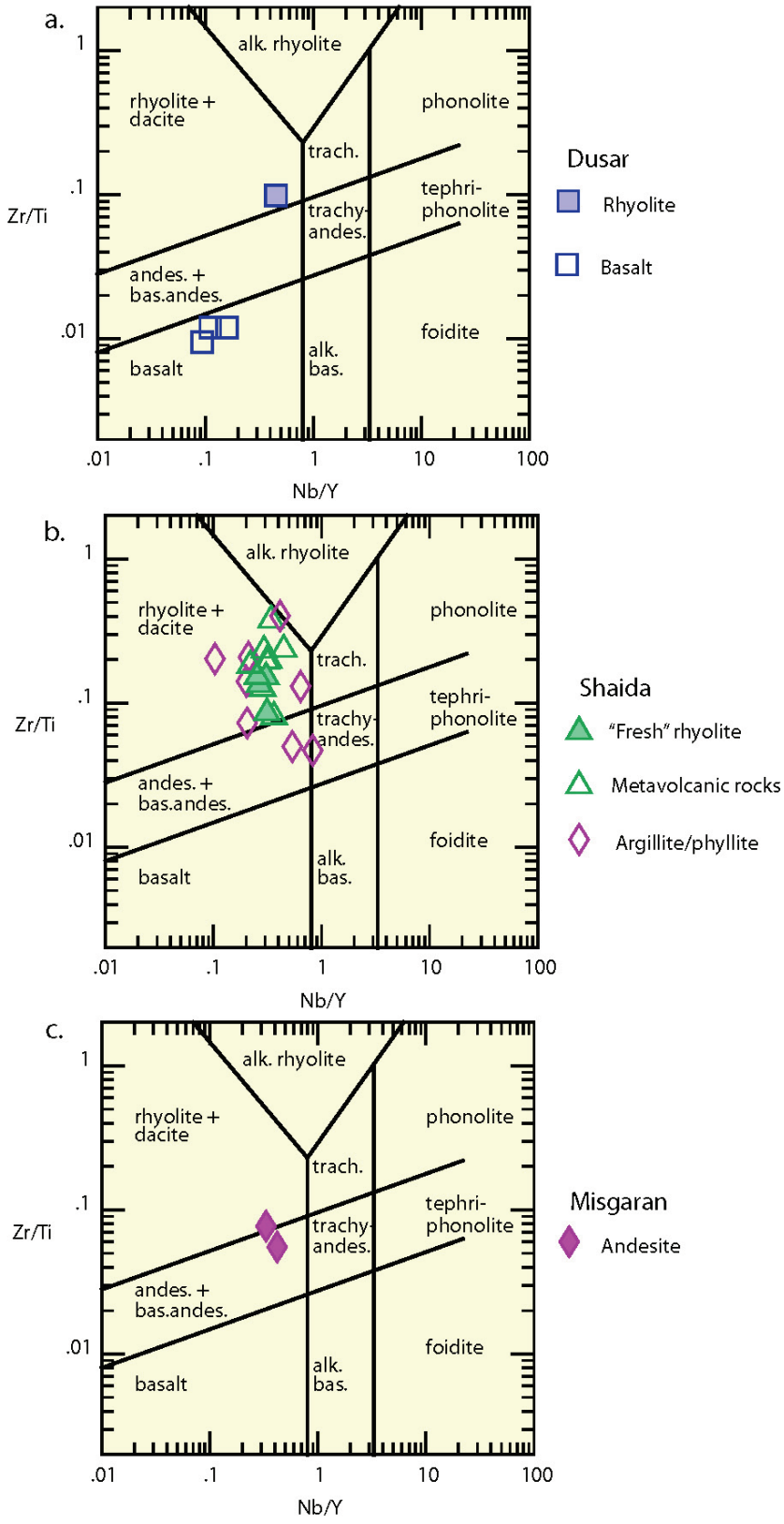

Figure 6A–8. Trace element discrimination diagram (Zr/Ti vs. Nb/Y) showing the classification of felsic, intermediate, and mafic metavolcanic rocks from the (a) Dusar, (b) Shaida, and (c) Misgaran subareas. Volcanic rocks in the Dusar subarea are of presumed Late Jurassic to Early Cretaceous age. Volcanic rocks from the Shaida and Misgaran subareas are of presumed Late Cretaceous age. Field boundaries after Pearce (1996) and Pearce and others (1984). Axes increments are unitless.

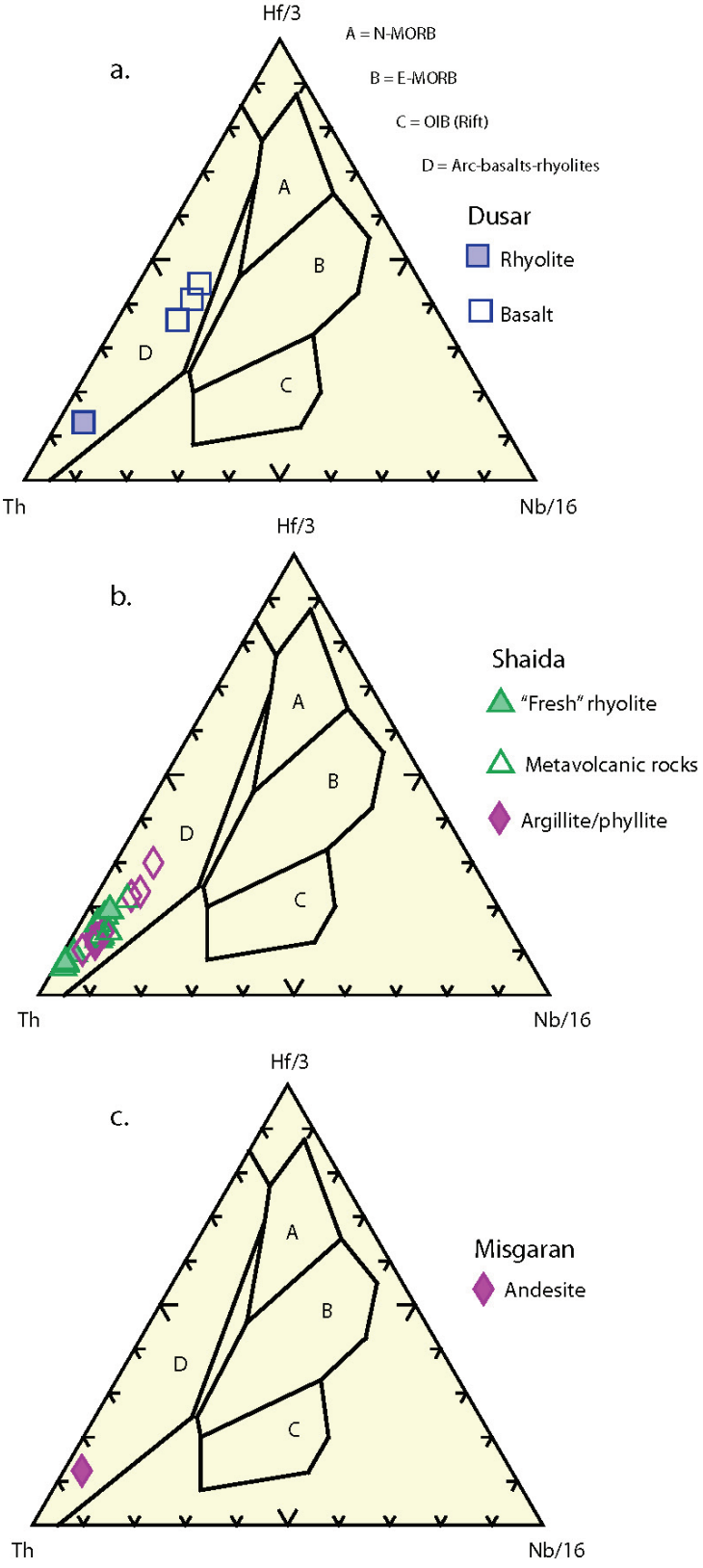

Figure 6A–9. Ternary trace element discrimination diagram (Hf, Th, Nb) showing the classification and inferred setting of felsic, intermediate, and mafic metavolcanic rocks from the (a) Dusar, (b) Shaida, and (c) Misgaran subareas. Volcanic rocks in the Dusar subarea are of presumed Late Jurassic to Early Cretaceous age. Volcanic rocks in the Shaida and Misgaran subareas are of presumed Late Cretaceous age. Field boundaries after Wood (1980). Axes ticks represent 10-percent increments.

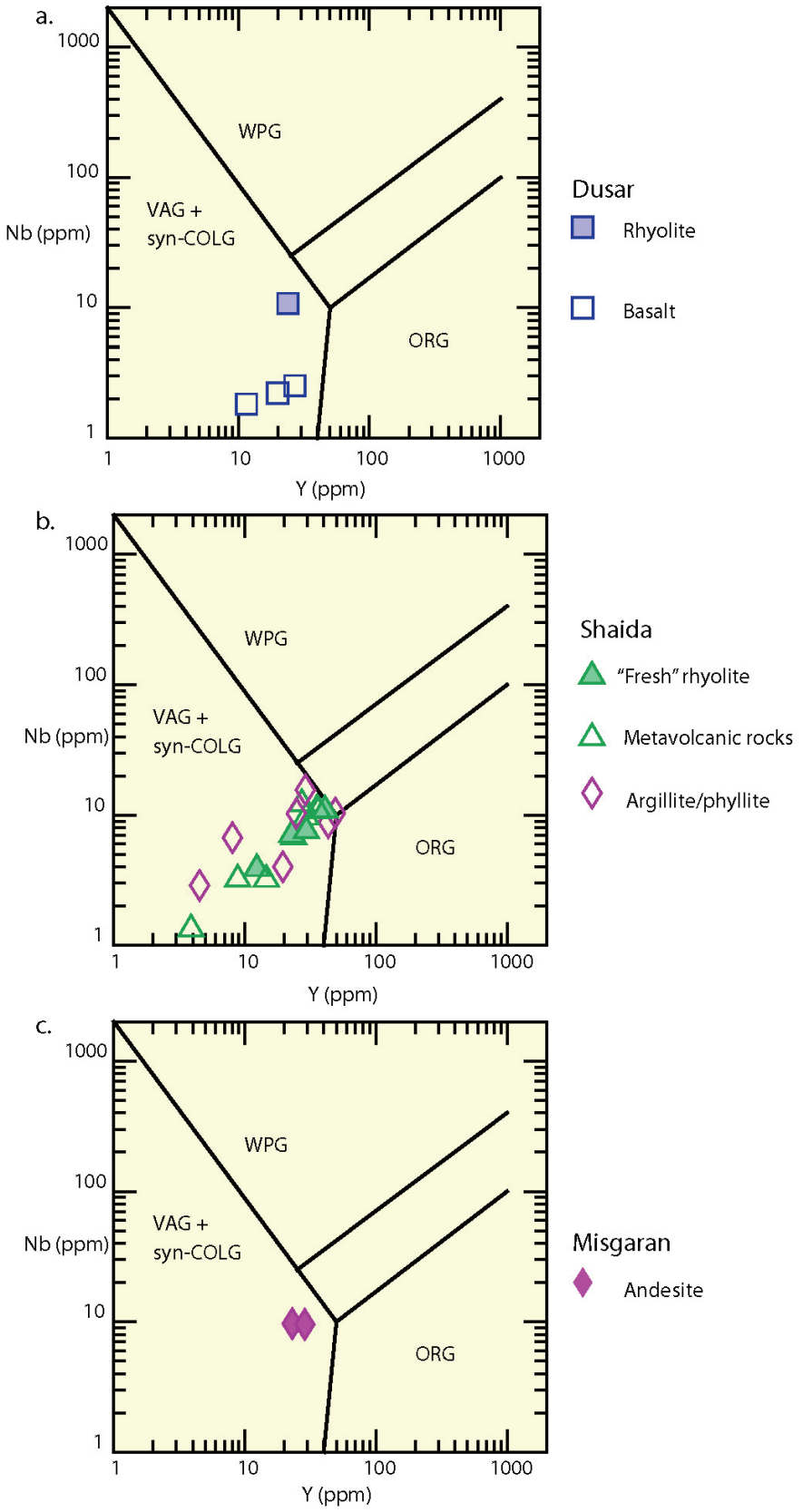

Figure 6A–10. Trace-element discrimination diagrams (Nb and Y) showing the classification an inferred setting of the metavolcanic rocks from the (a) Dusar, (b) Shaida, and (c) Misgaran subareas. Field boundaries after Pearce (1996) and Pearce and others (1984). The abbreviation ppm is parts per million.

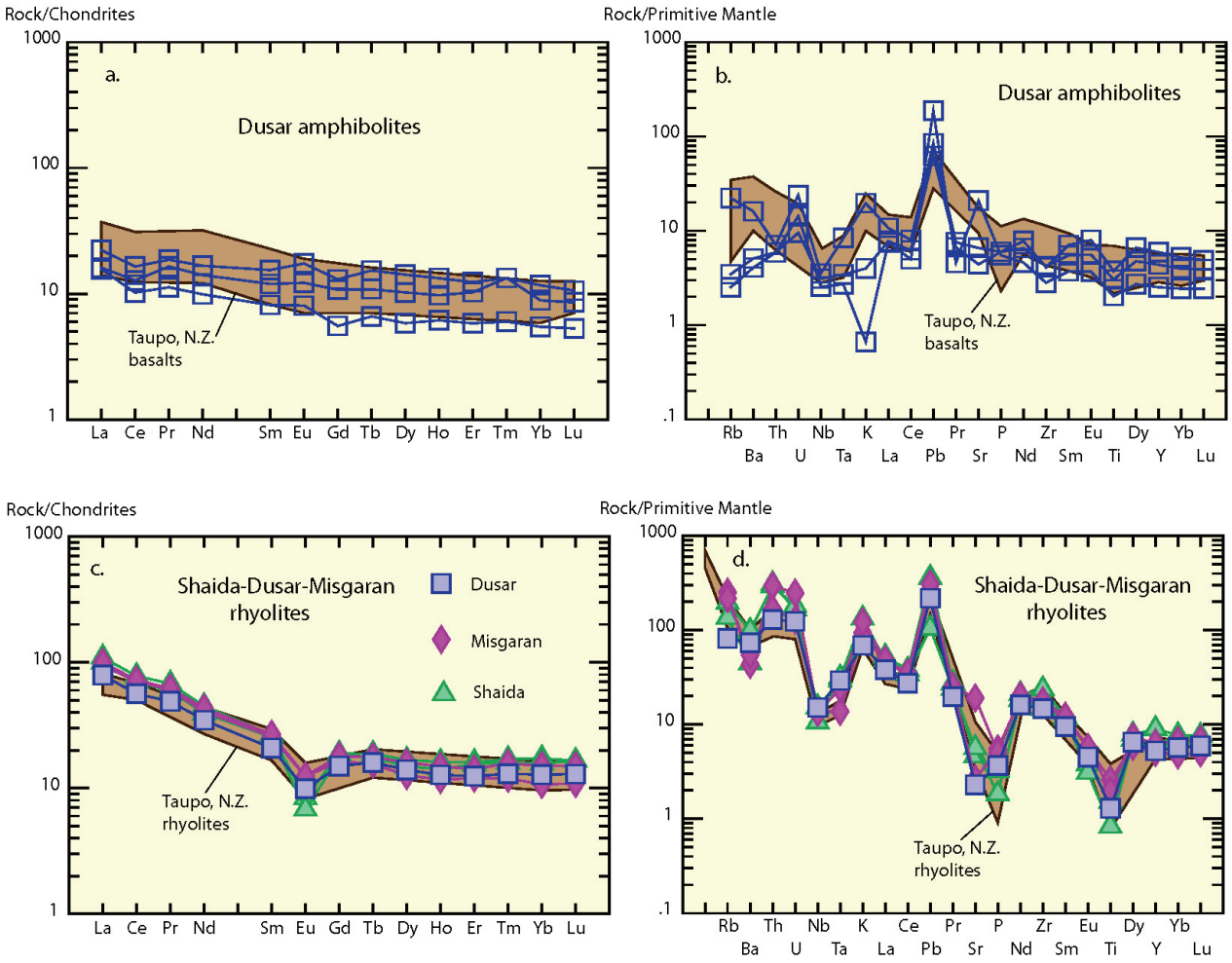

Figure 6A–11. (a) Rare earth element, and (b) trace element analyses of the Dusar amphibolites, normalized to (a) chondrites, and (b) primitive mantle. Also shown is the field for basalts (brown) from the Taupo volcanic zone, North Island, New Zealand (N.Z.). (c) Rare earth element and (d) trace element analyses of the felsic volcanic rocks from Dusar, Shaida, and Misgaran, normalized to (c) chondrites and (d) primitive mantle. Also shown is the field for rhyolites (brown) from the Taupo volcanic zone, North Island, New Zealand. Chondritic and primitive mantle values after Nakamura (1974) and Sun and McDonough (1989), respectively.

6A.5 Dusar Subarea Volcanic-Hosted Copper Prospects

The volcanic rocks in the Dusar subarea, of latest Jurassic (?) to Early Cretaceous age, are intruded by numerous diabase and gabbro intrusive bodies. The section of volcanic rocks is highly faulted and fractured, with two major gossans well developed above the volcanic rocks at the Dusar type locality, and Namak-sory.

6A.5.1 Dusar Gossan

The gossan is exposed as a north-south trending zone, approximately 1.5 km long and 200 m wide, consisting of discontinuous outcrops along a dry stream valley. Because of the brecciated nature of the gossan, its linear trend and low relief, we postulate that the gossan follows a paleofault or fracture zone. The gossan overlies with profound unconformity the Jurassic to Lower Cretaceous volcanic rocks, and is covered by unconsolidated Neogene sediments (fig. 6A–4*a*,*b*).

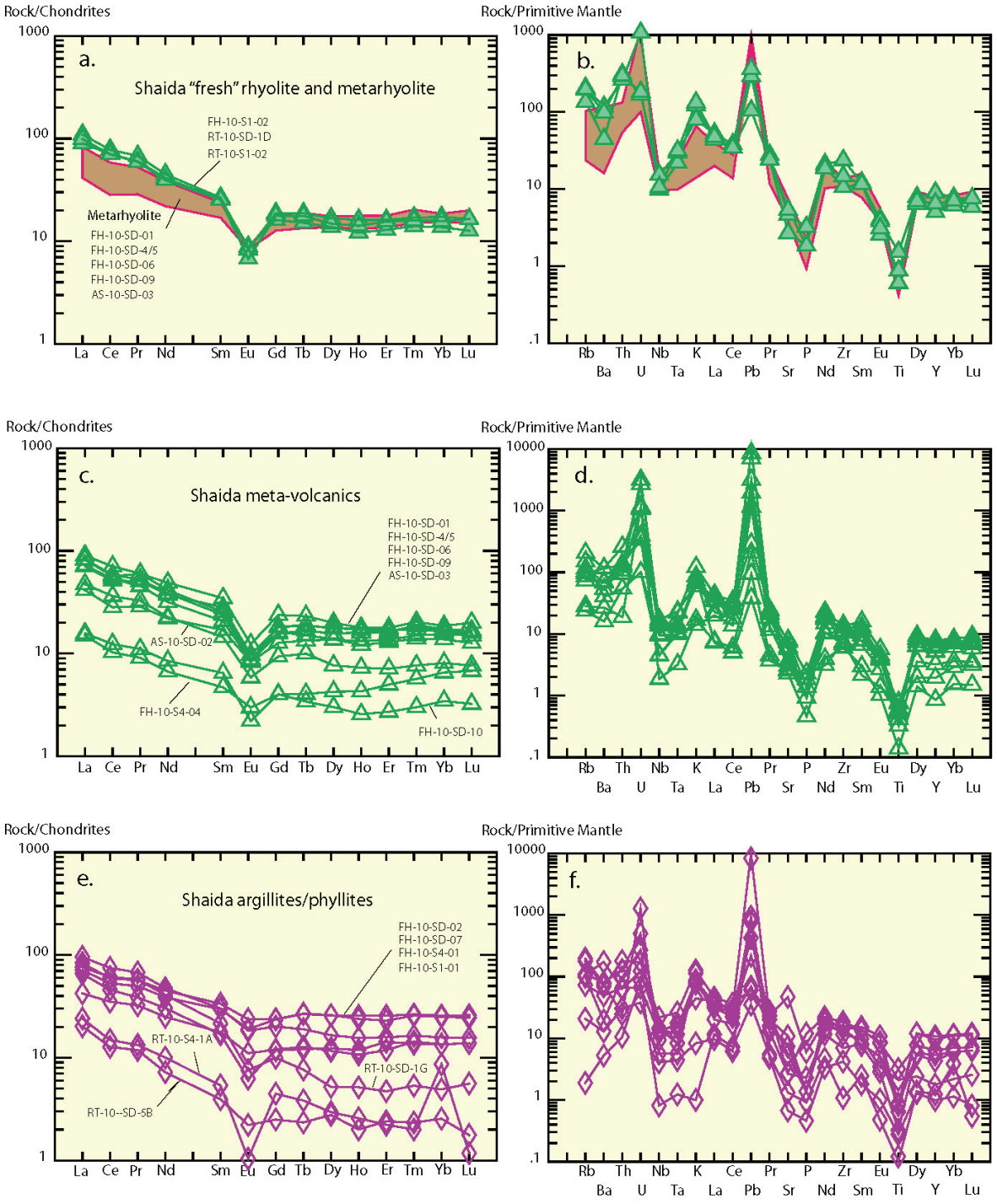

Figure 6A–12. Discrimination diagrams of the altered stratified rocks, gossans, and veins from the Dusar and Shaida subareas. Chondritic and primitive mantle values after Nakamura (1974) and Sun and McDonough (1989), respectively. Trace-element and rare earth element concentration values of basalts (brown) from the Taupo volcanic zone of New Zealand are from Gamble and others (1993). (a) Chondrite-normalized rare earth element (REE) diagram of the "fresh" volcanic and metavolcanic rocks from Shaida. (b) Rare earth element and trace element discrimination diagram of the "fresh" volcanic and metavolcanic rocks from Shaida. (c) Rare earth element variation diagram, normalized to chondrites, of altered metavolcanic rocks from the Shaida subarea. (d) Rare earth element and trace element discrimination diagram of the "altered" metavolcanic rocks from Shaida. (e) Rare earth element variation diagram, normalized to chondrites, of the altered argillites and phyllites from the Shaida subarea. (f) Rare earth element and trace-element discrimination diagram of the altered argillites and phyllites from Shaida.

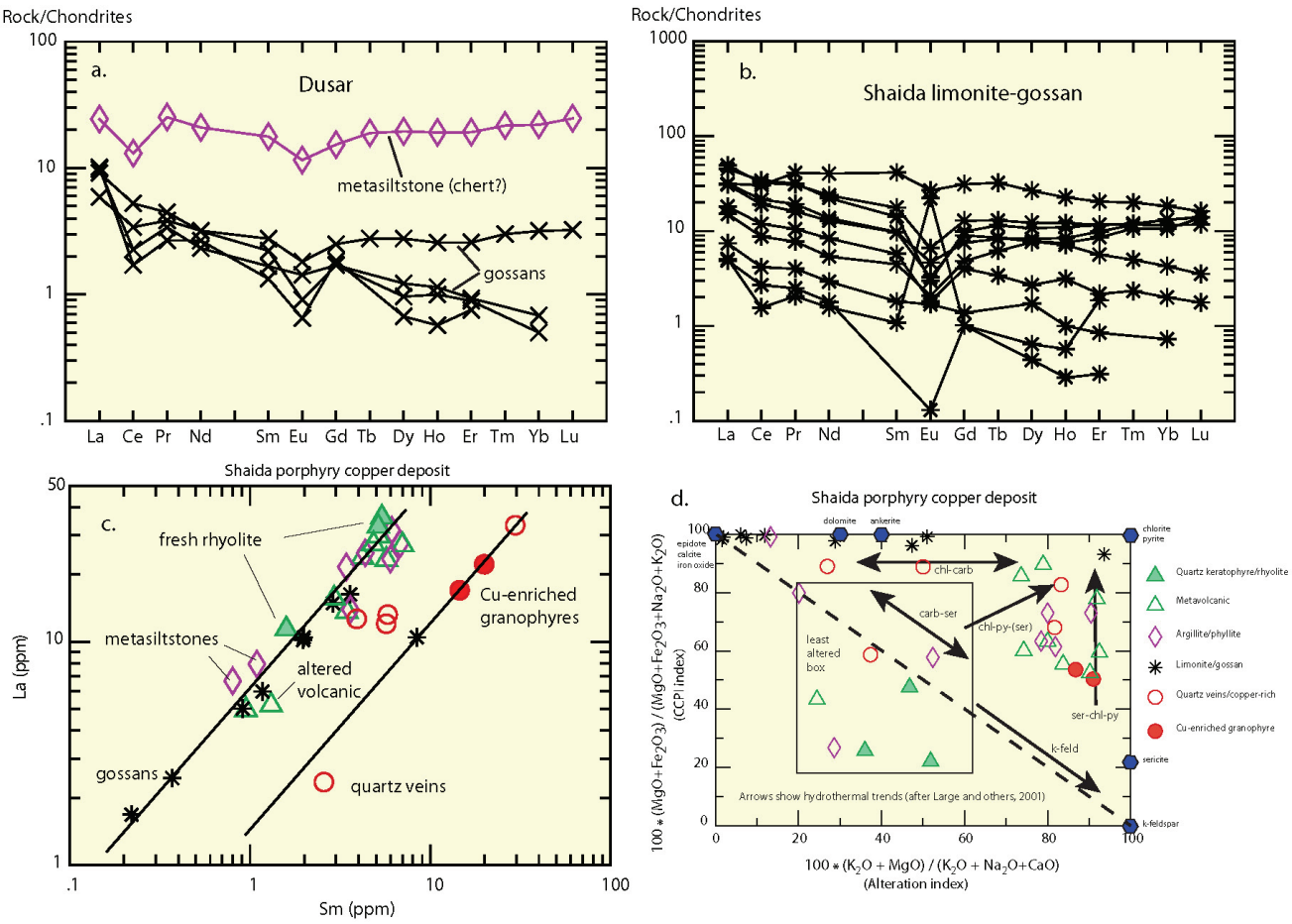

Figure 6A–13. Rare earth element variation diagram of the metasiltstone and gossans from the Dusar subarea, normalized to chondrites. Chondrite rare earth element (REE) abundances after Nakamura (1974). Note the low concentrations of REE in the gossans, and especially the relative heavy REE (LREE) depletions relative to the light REE (LREE). (b) Chondrite-normalized REE diagram of the limonite gossans from the Shaida subarea. Chondrite REE abundances after Nakamura (1974). (c) Log La compared to log Sm of the altered stratified rocks, copper mineralized granophyres, gossans, and quartz veins, of the Shaida district. (d) Alteration diagram of Large and others (2001) showing the analyses of the fresh metavolcanic and rhyolites from Shaida relative to the altered and mineralized samples from the Shaida district. The abbreviation ppm is parts per million.

The largest of the gossans at Dusar is approximately 2 km long and 30 to 200 m wide (fig. 6A–3 and 6A–4*b*). The thick mineralized zone consists of massive, ochreous, and siliceous limonitic gossan (fig. 6A–4*f*). According to Telkov and others (1972, 1973; cited by Abdullah and others, 1977), diamond drilling below the Dusar gossan intersected a siliceous and sericitic limonitic rock underlain by quartz keratophyre with disseminated pyrite. The mineralized sections grade 0.06 wt. % copper and up to 0.05 wt. % zinc; our assays of the Dusar gossan show anomalously high concentrations of arsenic and zinc (table 1), although not at the reported values of Telkov and others (1972). Additional mineral occurrences within this part of the tract contain geologically similar mineralized zones with anomalous concentrations of copper, zinc, and gold (Abdullah and others, 1977). The vein-like occurrences, some of which are up to 1.5 km long, are silicified and associated with diabase dikes that locally contain chalcopyrite and secondary copper minerals.

6A.5.2 Namak-Sory Gossan

The bedrock of the Namak-sory landing site is poorly exposed, and only a few localities were observed and sampled by U.S. Geological Survey (USGS) scientists. The gossan is visible as a small

knob, less than 100 m high, that rises above an alluvial plain of Neogene gravel. Elsewhere the gossan is buried beneath Neogene gravel and sandstone.

In addition to ground surveys, Telkov and others (1972) conducted both induced polarization and natural field-potential studies at the Namak-sory site (fig. 6A–3). Their survey indicated that the natural electric field potential varied little across the strike of the gossan, and thus the measured electric field could not be related directly to zones of sulfide mineralization. The method of induced polarization, however, yielded a different result. In that case, two isolated zones of sulfide mineralization were identified at Namak-sory. Zone 1 trends northwest-southeast, dips slightly to the southwest, is approximately 75 m thick, and extends to a depth of at least 100 m. Zone 2 trends northeast-southwest for 250 to 750 m, has a near-vertical dip along approximately 40 m of its length, and has an estimated width of 75 m.

The presence of thick, extensive gossans at Dusar and Namak-sory is suggestive of significant sulfide mineralization at depth. The composition of the mineralized volcanic rocks, and their association with shallow marine terrigenous sediments, is consistent with a volcanogenic origin, perhaps as a volcanogenic massive sulfide deposit in a continental back-arc setting

6A.6 Shaida Subarea Porphyry Copper-Zinc Occurrences

The Shaida subarea includes copper occurrences (lat 33°51'N., long 61°51'E.) hosted within Lower Cretaceous volcanic strata intruded by leucogranite and granite porphyry plugs of Late Cretaceous to Oligocene age (fig. 6A–5). The major zone of copper mineralization, the Shaida deposit (fig. 6A–5), coincides with a 200- to 300-m-wide, strongly fractured, limonitized and kaolinitized fault zone, where six steeply dipping mineralized bodies and a cupriferous pyrite gossan are present. The six bodies range between 150 and 850 m in length, and between 3 and 8 m in width; they consist of limonite, hematite, and minor secondary copper minerals assaying at 0.27 to 3.02 wt. % copper and 0.02 to 0.37 wt. % zinc (Abdullah and others, 1977). Based on diamond drilling (Tarasenko and others, 1973), the individual occurrences are between 1 and 10 m thick (averaging ~ 4 m) and up to 2,400 m long; they consist of pyrite, pyrrhotite, sphalerite, and minor chalcopyrite. Mineralization is in the form of massive veinlets and disseminated occurrences (fig. 6A–6*d*-*e*) that assay 0.04 to 1.6 wt. % copper (average 0.63 wt. % copper), 0.09 to 7.0 wt. % zinc (average 1.3 wt. % zinc), 0.01 to 0.5 wt. % lead (average 0.08 wt. % lead) and 0.2 to 0.03 grams per metric ton (g/t) gold. Calculated resources of 4.8 Mt (million metric tons) of ore assay 1.1 wt. % copper and 1.2 wt. % zinc.

6A.6.1 Shaida Deposit

The site designated as the Shaida deposit, is located in the southern part of the triangle-shaped area in figure 6A–5. Two abbreviated site visits, each less than 1 hour in duration, were made by the team of USGS scientists. The bedrock at both localities consists of highly fractured, silicified, and copper-oxide stained sericitic phyllite (metavolcanic and metasilt) intruded by thin (less than 4 m thick) sheets and dikes of leucogranite (fig. 6A–6*a*–*e*). At another locality within the Shaida deposit site, we noted a thick iron gossan (approximately 5 m thick), resting above brecciated phyllite heavily stained with Cu oxide minerals (fig. 6A–6*f*). Twenty-three samples were collected for geochemistry with several representative samples from the Soviet trenches that yielded ore-grade copper concentrations (20,000 to 60,000 parts per million) and anomalous concentrations of arsenic and zinc (table 2).

6A.6.2 Shaida 1

The site designated as Shaida 1 is located in the northern part of the triangle-shaped area (fig. 6A–5). It also is an area that was trenched by Soviet geologists in the 1970s. The bedrock at Shaida 1 consists of highly fractured, silicified, and copper-oxide stained sericite phyllite (metavolcanic and metasiltstone) extensively intruded by sheets and dikes of granite porphyry (fig. 6A–6*c*). Four samples were collected for geochemistry and isotopic dating; one of the samples collected for geochemistry was a malachite-stained phyllite with a Cu concentration of approximately 30,000 ppm.

6A.6.3 Shaida 4

Shaida 4 is located midway between the Shaida deposit and Shaida I sites, and within the subarea designated as having porphyry copper potential (fig. 6A–5). Several trenches, and a large iron gossan, were observed from the air.

Bedrock at the Shaida 4 site consists of extensively altered, mineralized and brecciated felsic volcanic and pelitic schist and phyllite. Also noteworthy was the presence of granite porphyry and quartz veins with syntaxial fiber growth, all extensively stained with copper-oxide (malachite). The exposure shares the general characteristics of the Shaida deposit and Shaida 4 sites.

6A.7 Misgaran Subarea Tin Skarn Occurrences

Porphyry copper deposits are typified by chalcopyrite and bornite, either disseminated or in veins and breccias, which are generally confined to the intrusive igneous rocks and immediate contact zone. If calcareous wall rocks are present, part of the deposit may occur as skarn, which is a high-temperature replacement of the carbonate country rock. Copper and tin skarn, which is observed around granitoids in the Misgaran subarea, commonly consists of veined and tabular masses of chalcopyrite, pyrite, cassiterite, hematite, and magnetite (and other copper sulfides) in a calc-silicate gangue.

The Misgaran subarea in Herat Province (lat 33°49′30″ N., long 61°06′E.) is defined by three tin-bearing mineral prospects associated with a moderate sized (approximately 50 km^2) Upper Cretaceous or Paleocene granite stock that intrudes Lower Cretaceous sandstone, siltstone, shale, and limestone (figs. 6A–5 and 6A–6). The mineralization may be traced over a large zone, approximately 12 km^2, approximately 2.5 km long and 50 to 300 m wide. Two vein and stockwork prospects are closely adjacent to the stock, and all are characterized by quartz-tourmaline alteration. The most extensive zone of mineralization, about 3 km east of the stock, is a tin-bearing polymetallic skarn having alteration beds as much as is 950 m long, 460 m thick, and up to 300 m thick (fig. 6A–6). Mineralization also takes the form of numerous subparallel veins and nests with lead-zinc sulfide minerals and cassiterite. Tin is present as disseminated sulfides and stannite associated with galena. The tin concentration commonly grades between 0.01 and 6.0 weight percent and averages less than 0.11 weight percent. Associated base metals, lead and copper, commonly occur in trace amounts (Kabakov, 1973). The thickness and widespread nature of the mineralization suggests that the area could contain a large skarn deposit.

The presence of three partially explored tin-bearing magmatic-hydrothermal systems and the widespread occurrence of geochemical halos indicate the possible presence of undiscovered tin deposits. Uncertainty about the deposit type—vein, stockwork greisen, porphyry, skarn, or replacement—prevents making a quantitative estimate of potential resources.

6A.8 Summary of Potential

The presence of relatively well-explored copper- and zinc- bearing prospects in the Farah Rod Area of Interest and its subareas is an important positive indicator for a deposit of commercial size in this area. The geologic and petrologic characteristics of the associated igneous rocks, and the available assays, suggest two different types of deposits in the region.

Mineralization in the Dusar subarea has characteristics compatible with the descriptive volcanogenic massive sulfide (VMS) model, perhaps in a continental back-arc setting. Many of the occurrence descriptions indicate significant gossanous zones. There are promising assays from the district, and the geophysical work conducted by the Soviets in 1971 revealed that the Namak-sory site is prospective for sulfide ores. The position of the mineralized zones at Namak-sory was ascertained and, in 1972, the Soviets drilled several holes (Telkov and others, 1973). Borehole number 1 at the Namak-sory site exposed extensive pyrite mineralization, but extensive mineralization was not found at the Dusar site.

The Shaida subarea is properly classified as a highly prospective copper porphyry deposit. The zone of copper mineralization coincides with a 200- to 300-m-wide, strongly fractured, limonitized and kaolinitized fault zone, where six steeply dipping mineralized bodies and a cupriferous pyrite gossan are

present. The main zone of mineralization, 2.6 km long and 300 to 500 m wide, consists of secondary copper minerals assaying 0.27 to 3.02 wt. % copper and 0.02 to 0.37 wt. % zinc. The grade of these ores was confirmed by the USGS sampling team in August 2010. Based on diamond drilling (Tarasenko and others, 1973), the individual occurrences are between 1 and10 m thick (averaging approximately 4 m) and are up to 2,400 m long. The mineral occurrences consist of pyrite, pyrrhotite, sphalerite, and minor chalcopyrite in massive veinlets and disseminated ores that assay between 0.04 and 1.6 wt. % copper (average 0.63 wt. % copper), between 0.09 and 7.0 wt. % zinc (average 1.3 wt. % zinc), between 0.01 and 0.5 wt. % lead (average 0.08 wt. % lead), and between 0.2 and 0.03 g/t gold. Calculated resources are 4.8 million metric tons (Mt) of ore assaying 1.1 wt. % copper and 1.2 wt. % zinc.

Although not visited by the USGS sampling team, the Misgaran tin occurrence is also rated as modestly prospective. The occurrence is defined by three tin-bearing mineral prospects of modest size (approximately 50 km^2) within a Late Cretaceous or Paleocene granite stock that intrudes Early Cretaceous sandstone, siltstone, shale, and limestone. The mineralization is traceable over a large area, approximately 12 km^2, that is 2.5 km long and between 50 to 300 m wide. The most extensive zone of mineralization, about 3 km east of the stock, is a tin-bearing polymetallic skarn having alteration beds as much as is 950 m long, 460 m thick, and up to 300 m thick. Reported tin assays have high potential, with tin concentrations ranging between 0.01 and 6.0 weight percent and averaging less than 0.11 weight percent (Kababakov, 1973; Khasanov and others, 1967).

Future discoveries and definitions of resources will require extensive field examination and geophysical surveys. Ground surveys should be done in concert with detailed mapping and geochemical sampling, including trenching and drilling. In addition, extensive geophysical exploration, including low-elevation aeromagnetic, electroconductivity, and aeroradiometric surveys, must accompany the next round of field work. Such exploration could delineate defined zones of mineralization, sufficient in grade and size, for future commercial development.

6A.9 References Cited

Abdullah, S., Chmiriov, V.M., Stazhilo-Alekseev, K.F., Dronov, V.I., Kofarsky, A.K., and Malyarov, E.P., 1977, Mineral Resources of Afghanistan: Republic of Afghanistan, Ministry of Mines and Industries, Afghan Geological and Mines Survey, 419 p.

Afghanistan Geological Survey, 2006, The potential for copper: Afghanistan Geological Survey website, accessed Sept. 1, 2006, at *http://www.bgs.ac.uk/afghanminerals/mininfo.htm*.

Balance, P.F., 1976, Evolution of the Upper Cenozoic magmatic arc and plate boundary in northern New Zealand: Earth and Planetary Science Letters 28, no. 3, p. 356–370.

Debon, F., Afzalie, H., Lefort, P., and Sonnet, J., 1987, Major intrusive stages in Afghanistan—typology, age, and geodynamic setting: Geologische Rundschau, v. 76, p. 245–264.

Doebrich, J.L., Wahl, R.R., Ludington, S.D., Chirico, P.G., Wandrey, C.J., Bohannon, R.G., Orris, G.J., Bliss, J.D., 2006, Geologic and mineral resources map of Afghanistan: U.S. Geological Survey Open–File Report 2005–1038, scale 1:850,000, accessed Sept. 1, 2006, at *http://pubs.er.usgs.gov/usgspubs/ofr/ofr20061038*.

Gamble, J.A., Smith, I.E.M., McCulloch, M.T., Graham, I.J., and Kokelar, B.P., 1993, The geochemistry and petrogenesis of basalts from the Taupo Volcanic Zone and Kermadec Island Arc, S.W. Pacific: Journal of Volcanology and geothermal Research, v. 54, p. 265–290.

Kabakov ,O.N., 1973, Tin occurrences in Afghanistan: Summary report by the prospecting and evaluating team on the work in 1970–1972: Ministry of Mines and Industries, Kabul, Rec. Off. Department of Geology and Mines, 1973.

Khasanov, R.M., Plotnikov, G.I., Bayazitov, R., Sayapin, V.I., and Trifonov, A., 1967, Report on revised estimation investigations of mineral deposits and occurrences of copper, lead, zinc and gold in 1965– V. I–II: Department of Geological and Mineral Survey, Kabul, unpub. data.

Large, R.R., Gemmell, J.B., Paulick, Holger, and Huston, D.L., 2001, The alteration boxplot: A simple approach to understanding the relationship between alteration mineralogy and lithogeochemistry associated with volcanic-hosted massive sulphide deposits: Economic Geology, v. 96, p. 957–971.

Leroy, J.L., and Turpin, Laurent, 1988, REE, Th and U behavior during hydrothermal and supergene processes in a granitic environment: Chemical Geology, v. 68, p. 239 251.

Nakamura, N., 1974, Determination of REE, Ba, Fe, Mg, Na and K in carbonaceous and ordinary chondrites: Geochimica et Cosmochimica Acta v. 38, no. 5, p. 757–775.

Metal Mining Agency of Japan (MMAJ), 1998, Mineral Resources Map of Asia: Metal Mining Agency of Japan map, 43 p., 1 sheet, scale 1:10,000,000.

Orris, G.J., and Bliss, J.D., 2002, Mines and Mineral Occurrences of Afghanistan: U.S. Geological Survey Open-File Report 2002–110, 95 p., accessed Sept. 1, 2006, at *http://geopubs.wr.usgs.gov/open–file/of02–110/.*

Pearce, J.A., 1996, A user's guide to basalt discrimination diagrams, *in* Wyman, D.A., ed., Trace element geochemistry of volcanic rocks: Applications for massive sulphide exploration: Geological Association of Canada, Short Coarse Notes v. 12, p. 79–113.

Pearce, J.A., Harris, N.B.W., and Tindle, A.G., 1984, Trace element discrimination diagrams for the tectonic interpretation of granitic rocks: Journal of Petrology, v. 25, p. 956–983.

Peters, S.G., Ludington, S.D., Orris, G.J., Sutphin, D.M., Bliss, J.D., and Rytuba, J.J., eds., and the U.S. Geological Survey Afghanistan Ministry of Mines Joint Mineral Resource Assessment team, 2007, Preliminary non-fuel mineral resource of Afghanistan: U.S. Geological Survey Open-File Report 2007–1214, 810 p., 1 CD–ROM and available online at *http://pubs.usgs.afghanminerals.*

Plotnikov, G.I., and Slozhenikin, A.P., 1968, Report on the results and revised evaluation work of copper, lead–zinc, and gold occurrences in Afghanistan carried out in 1967: Department of Geological and Mineral Survey, Kabul, unpub. data.

Singer, D.A., Berger, V.I., and Moring, B.C., 2005, Porphyry Copper Deposits of the World—Database, Map, and Grade and Tonnage Models: U.S. Geological Survey Open-File Report 2002–1060, available online at *http://pubs.usgs.gov/of/2005/1060/.*

Sun, S.S., and Mc Donough, W.E., 1989, Chemical and isotopic systematics of oceanic basalts: Implications for mantle composition and processes: Geological Society Special Publication, v. 42, p. 313–345.

Tarasenko V.I., Kovalenko A.C., Arwanitaki S.B., Borozenets N.I., 1973, Report on the results of geological prospecting and survey for copper and base metals carried out by the Andreskan and Dusar teams in Western Afghanistan in 1971–1972: Department of Geological and Mineral Survey, Kabul, unpub. data.

Telkov, V.S., Burenin, D.O., Kamaev, S.V., and Kleimenov, M.A., 1972, Report on the geological survey for solid minerals conducted in 1971: Ministry of Mines and Industries, Department of Geology and Mines, Kabul Afghanistan, 43 p. plus annexes.

Telkov, V.S., Kamaev, S.V., Kleimenov, M.A., and Semyonov, v.S., 1973, Report on the geological survey for solid minerals conducted in 1972: Ministry of Mines and Industries, Department of Geology and Mines, Kabul Afghanistan, 76 p.

United Nations Economic and Social Commission for Asia and the Pacific (ESCAP), 1995, Atlas of mineral resources of the ESCAP region—Geology and mineral resources of Afghanistan: United Nations Economic and Social Commission for Asia and the Pacific, 150 p. [Available from the National Technical Information Service, Springfield, Va., as NTIS Report UN–0561.]

Wood, D.A., 1980, The application of a Th-Hf-Ta diagram to problems of tectonomagmatic classification and establishing the nature of crustal contamination of basaltic lavas of the British Tertiary volcanic province: Earth and Planetary Science Letters, v. 50, p. 11–30.